ARTECH CORP.
14554 Lee Road • Chantilly, Virginia 22021-1632
(703) 378-7263 • Washington, D.C. Metro 968-TEST • Fax (703) 378-7274

# FRACTOGRAPHIC AND MICROSTRUCTURAL EXAMINATION OF A RUPTURED DOT-3AL SPECIFICATION COMPRESSED GAS CYLINDER

BY

Vishwanath Sahay
Paul J. Lare

July 27, 1995

Prepared for:

U.S. DOT/RSPA/
400 7th Street, S.W.
Washington, D.C. 20590-0001

Order No. DTRS56-95-P-70149

ARTECH File No. 9509.004

## TABLE OF CONTENTS

## INTRODUCTION

This report details microstructural and fractographic analysis of the segments of a DOT E-6498-2216 ruptured cylinder. Reportedly, the cylinder had failed in 18 pieces while being refilled. The subject cylinder was made from Al6351 aluminum alloy under Exemption 6498 and marked in accordance with 49 CFR Part 178.46. The cylinder was manufactured by Luxfer USA for Scott Aviation; date of manufacture: 9-1980. One fractured piece of an exemplar cylinder was also provided for comparison analysis. As reported, this cylinder was made similar to the subject cylinder; it had been in service for 10-12 years. The cylinder had been over-pressurized to failure; over-pressurization exceeded the design burst pressure. No other details of this cylinder are available at this time.

Analysis was performed under the direction of the DOT COTR.

## SAMPLE DESCRIPTION

The major pieces of the exploded pressure cylinder are shown in Figure 1, in a best fit arrangement, that was based on the center nine (9) pieces (Figure 2) having been one continuous piece that had been analyzed previously. The remaining major pieces were then arranged on the basis of exterior and interior surface features and fracture profiles, as indicated in Figure 3.

Exterior and interior surfaces of the nine (9) sectional pieces comprising Figure 2 are shown in the as-received condition in Figures 4 through 8, and the remaining seven (7) major

fracture pieces are shown in Figures 9 through 13, also in the as-received condition. Ten fracture fragments, shown in Figure 14 in the as-received condition, could not be located in the arrangement of pieces (Figure 1) due to their small size and fracture surface damage. Figure 15 details the as-received condition of the valve as having corroded, deformed, and several sheared threads, the "O" ring seal, and the over-pressurizing rupture disc protection mechanism. Identification markings from the heavy wall area of the top of the cylinder are shown in Figure 16. The significance of the letter "A" following "Lot Code X59" and the unidentifiable symbol to the left of "X59A" is not known at this time (Figure 17). Enlarged views of the as-received condition of the threaded areas of the fracture pieces (2), (4), and (1I) are shown in Figure 18, revealing additional cracks in the interior formed surface of the neck and in the more corroded areas of the threads.

For comparison with the exploded cylinder material, a small section of an exemplar cylinder(Figure 19) was provided, wherein the exemplar cylinder had been burst tested in excess of the design burst pressure. The extent of over-pressurization is not known at this time.

## FRACTURE EXAMINATION OF THE SUBJECT CYLINDER

Subsequent to visual examination of the fractured pieces, selected fracture surfaces were examined under optical and scanning electron microscope (SEM).

FRACTURE SURFACE #1 - The fracture section was retrieved from the neck region of the cylinder, shown earlier in the report. A macro view of the fracture surface is presented in Figure 20. The failure appeared to have initiated on the inside surface in the thick region near the neck. The fracture section was solvent-cleaned using standard laboratory practices. Optical microscopic examination at higher magnifications revealed the presence of a considerably large population of dark streaks all over the fracture surface (Figure 21). These streaks were thin slender voids having textured surfaces as depicted in the SEM micrograph in Figure 22. Examination of several of these voids suggests that chunks of dross* had been entrapped in the material at various locations during manufacturing and voids had formed at those locations when the mass of dross dislodged or pulled out during the fracture process. It should be noted that the presence of dross in the material is detrimental to its physical properties.

SEM micrographs exhibiting typical fracture features at locations noted in Figure 20 are presented in Figures 23-32. Note that locations 1-5 are in the region having large grain structure (refer to the microstructural examination section of this report).

Figure 23. The shape and orientation of dimples shown in the fractograph taken at location 1 indicate that the failure initiated in the threads in tearing mode

* Dross is a metal oxide inclusion.

due to overload and progressed inward.

Figure 24. The fractograph appeared to be featureless. Some overload dimples were also observed.

Figures 25. & 26. The fractographs show similar characteristics as in Figure 24.

Figure 27. It exhibits featureless facets as in Figures 24-26. The failure is still due to overload. The fracture initiated along the metal fold on the inside surface, formed during manufacturing process.

Figures 28. & 29. These fractographs are taken from the regions having finer grain structure. The failure mode is typical of overload. Unlike featureless facets in Figures 24-27, a relatively larger number of dimples was observed.

Figures 30. & 31. The fractographs are from locations 8 and 9 respectively. They show a mixed mode of fracture consisting of dimples and intergranular failure. Both features are indicative of failure due to overload.

Figure 32. Fractograph from the shiny edge of the fracture exhibits features of shear overload failure.

FRACTURE SURFACE #2 - A section from the neck region containing threads was removed from the piece shown in Figure 8. An

undisturbed view of the inside surface of the section is presented in Figure 33. Notice crack-like features in the threads as well as on the adjacent internal surface. A through-thickness saw cut was made along the dotted line shown in Figure 33a. A fresh fracture was created by flexing the remaining ligament; the newly created fracture contained the crack-like feature shown in Figure 33b. An enlarged view of the lab-created fracture surface is presented in Figure 34. The crack-like feature was about 0.017 inch deep. Its color was similar to the rest of the inside surface of the cylinder which suggests that the crack was formed during the manufacturing process. The presence of such cracks is detrimental to integrity of the cylinder because they offer a ready site for cracks to propagate under favorable stress conditions.

SEM micrographs exhibiting fracture features at locations indicated in Figure 34 are shown in Figures 35-37; these fractographs were taken from the region having large grain structure.

Figure 35. Fractograph shows featureless facets as exhibited in Figures 24-27; smoothness of these facets suggests that there was no interfacial cohesion in those areas. Fractograph also shows some areas having dimpled rupture.

Figure 36. It shows similar features as in Figure 35.

Figure 37. Fractograph exhibits featureless facets and some

dimpled ruptures. A semi-quantitative chemical analysis, using energy dispersive spectroscopy (EDS), of the particle-like object in the micrograph was performed and result was compared with that of the matrix. No difference in chemical composition was detected. Similarity between the two chemistries suggests that the particle is part of dross which was entrapped in the material during manufacturing.

## FRACTURE EXAMINATION OF THE EXEMPLAR CYLINDER

An as-received view of the fracture surface is presented in Figure 38. Because it was badly contaminated, it had to undergo extensive cleaning prior to examination. Unlike the subject cylinder, the material of the exemplar cylinder was almost free from dross and voids. See Figure 39; compare this Figure to Figure 21. SEM examination revealed that the mode of failure was similar to that of the subject cylinder; it exhibited typical features of overload fracture (Figure 40). The featureless facets seen in Figures 24-27 and 35-37 were not observed on the exemplar fracture surface.

## MICROSTRUCTURAL EXAMINATION

Prior to initiation of the microstructural examination X-ray radiographs were taken of the thick-wall fracture pieces to locate any detectable injurious subsurface defects that could

affect the structural integrity of the cylinder. Shown in Figure 41 is a positive print of an X-ray radiograph of fracture piece (4) in which several indications could not be related to surface damage. A transverse section was taken through the indication closest to a longitudinal fracture for metallographic comparison with a transverse section from the exemplar fracture sample. The sections were metallographically prepared in accordance with the standard practices of ASTM E3. As can be observed in Figure 42, the as-polished surface contains a relatively higher and more elongated inclusion content than observed for the exemplar surface. This observation was made on the basis of utilizing several metallograph preparation procedures and polishing materials to evaluate possible polishing artifact complicity.

To evaluate the cause of fragmenting of the subject cylinder into eighteen (18) pieces, metallographic sections were taken in and around the threaded, heavy-wall area as well as from the thinner wall areas having longitudinal and transverse fractures. Shown in Figures 43-46 are examples of dross entrapment that were found in all sections except for the singular exemplar fracture sample. As a result, all fracture surfaces were examined at magnifications of 7X to 40X with a stereoscopic microscope, and all fracture surfaces were found to contain delaminated segments of dross that varied in thickness and length.

Susceptibility to intergranular corrosion was also examined after finding evidence of this mechanism at a localized spot on the interior surface in the area of angular transition of the

bottom to the side wall, as can be seen in Figure 47. Further evidence of this attack was found along the length of the thread though not as a continuous process, as indicated in Figures 48 and 49. Evidence of cold work on the upper portion of the thread (Figure 49) suggests that a thread mismatch, such as a tapered metric thread might produce, may have occurred at some point in the cylinder's service lifetime.

Microstructural variation was found in the thickest wall section adjacent to the threaded hole. At the wrinkled internal surface, cracks were found to emanate from radial surface texture notches (Figure 50) that were produced during thermal-mechanical forming of the top of the cylinder. A relatively high inclusion content appeared to be dispersed in a large recrystallized grain structure. At the level of the bottom thread a slight increase in microconstituent alignment was observed (Figure 51). A highly aligned microstructure with very large, elongated grains was found at the level of the top thread (Figure 52). Also observed within the thick wall area of the threaded hole were several places in which a stacking or pile-up of microconstituents and unidentified inclusions occurred, as shown in Figure 53.

## DISCUSSION

Fractographic examination of the failure suggests that the failure was catastrophic and occurred due to overload conditions. The overload conditions may have been created either by over-pressurization or inherent weakness due structural anomalies in

the material. Evidence of structural anomalies found were -

a.) A large population of voids on the fracture surfaces

b.) The presence of smooth/featureless facets on the fracture face near the inside surface in the neck region. These facets are areas where there was a complete lack of interfacial cohesion. These are a kind of discontinuity which was carried over from casting of the raw material blank to manufacture of the cylinder. Most likely, the discontinuity would be in the form of shrinkage which can exist as a region of interdendritic void(s) sometimes associated with suspended dross, during the various stages of solidification. When extruded, to form the cylindrical precursor to the final product, the shrinkage/dross volume compresses and realigns in accordance with flow constraints of the metal, due sealing or healing of the void cannot occur because of the oxide skin of the void and/or the presence of dross. Obviously, the higher the content of the dross in the cast billet blanks, the poorer will be the mechanical properties of the final product, with transverse properties being more affected than longitudinal properties due to the realignment and distribution of the dross. Furthermore, the observed microstructural variation in the thick wall region adjacent to the threads suggests a mechanical response that may additionally reduce the transverse properties to the levels less than the design properties.

The presence of radially oriented surface notches on the interior surface at the bottom of the threaded hole presents

potential sites for corrosion activity. The deterioration of the threads by corrosion, however it occurred, raises the question of whether or not the valve can be explosively ejected.

## CONCLUSIONS

The following conclusions are drawn on the basis of the findings and observations relating to the sample material contained herein:

1. The quality of the manufactured cylinder that fragmented is poor due to the presence of excessive detrimental dross content which was not found in the exemplar fracture sample.
2. The high detrimental dross content severely reduces the transverse properties that result in significantly reduced toughness and increased likelihood of fragmentation on pressurizing.
3. Corrosion of the threads and evidence of thread mismatch may have influenced the service life of the cylinder.

## RECOMMENDATIONS

1. Analyze unidentified microconstituents/inclusions, conduct trace element analyses, and analyze corrosion product(s) to assess potential involvement in loss of structural integrity in manufactured pressure cylinders.

2. Determine transverse mechanical properties of the heavy wall material adjacent to the threaded hole for the fragmented and the exemplar cylinder.
3. Calculate the burst pressure from the bulge of the unruptured disc.
4. A statistically significant number of failed cylinders should be examined to draw a correlation among causes of failures.
5. Consideration should be given toward establishing an evaluation program to determine the remaining life and/or safe (risk-free) operation of existing cylinders manufactured under exemption and DOT 3AL 3000, incorporating the following elements:
    A. DOT collection of a statistically significant number of cylinders with manufacturing and inspection records and certifications.
    B. X-ray radiography and visual inspection of threaded hole and internal surface of heavy wall area.
    C. Pressure cycling and burst testing at several levels of cycling.
    D. Examine and characterize failures.
    E. Characterize chemical and transverse mechanical properties.
    F. Analyze data for predictability of failures.
6. Stress analysis of original design parameters.

7. Recommendations listed above may be useful for a policy decision aimed at regulating such cylinders still in service.

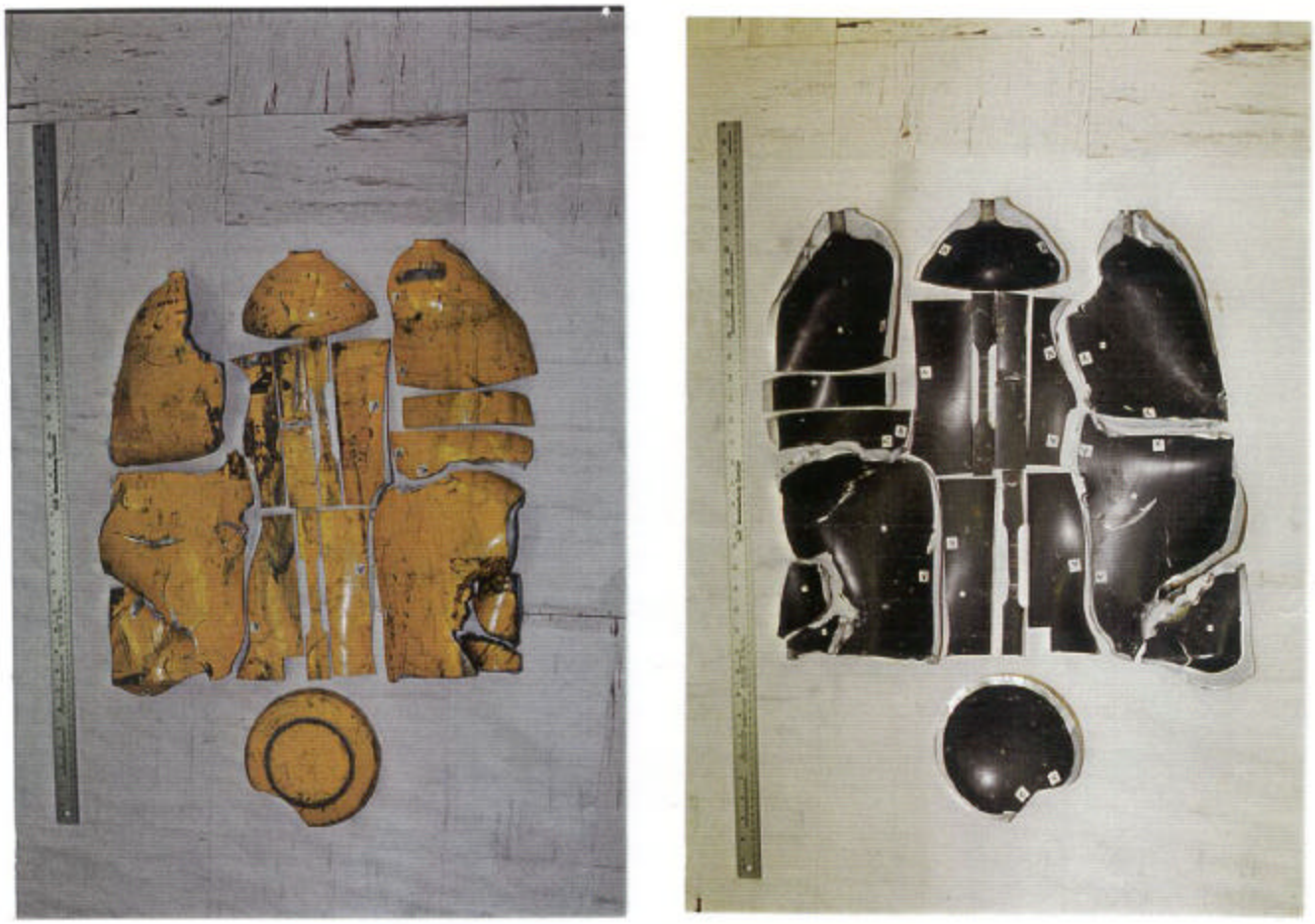

Figure 1. Major pieces of exploded air pressurized (SCUBA) cylinder E6498-2216. Caret marks indicate clearly defined chevron patterns that point to the fracture origins.

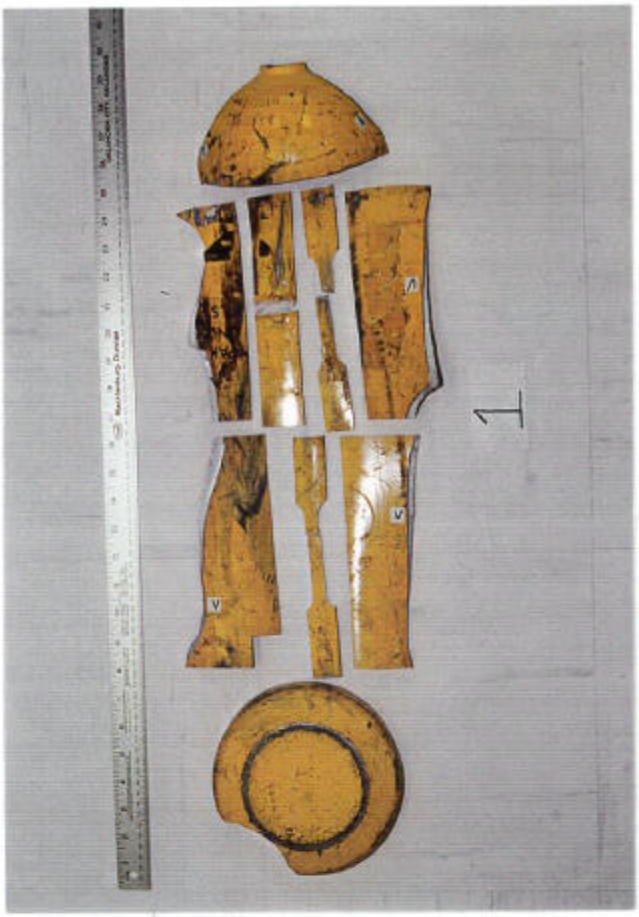

Figure 2. Arrangement of test coupons, from a previous examination, which constitutes one continuous failure section.

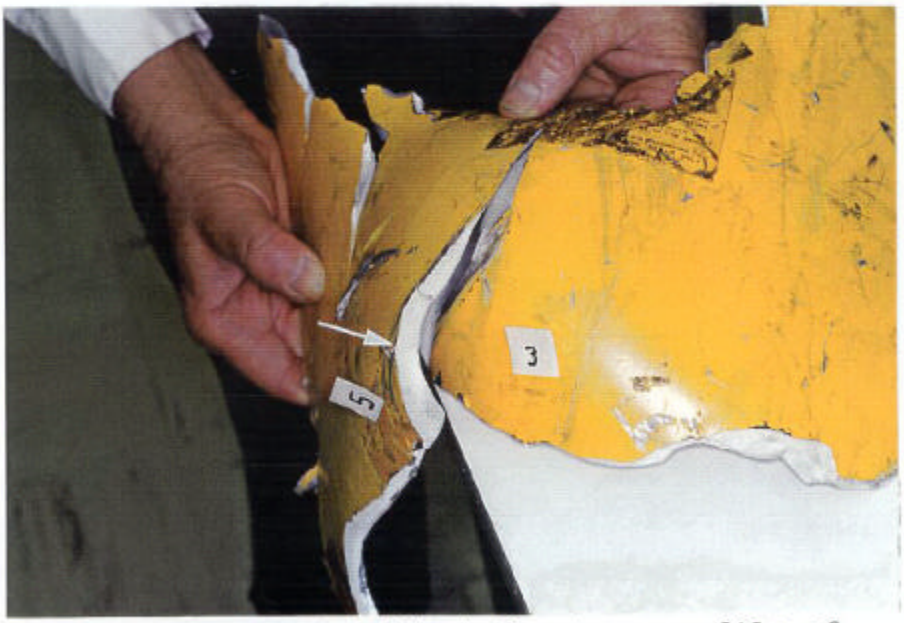


Figure 3. Matching (without touching) fracture profile of fracture piece #3 with #5. Arrow locates the only flat, 90° fracture area (approx. 1 inch long) within the cylindrical wall area.

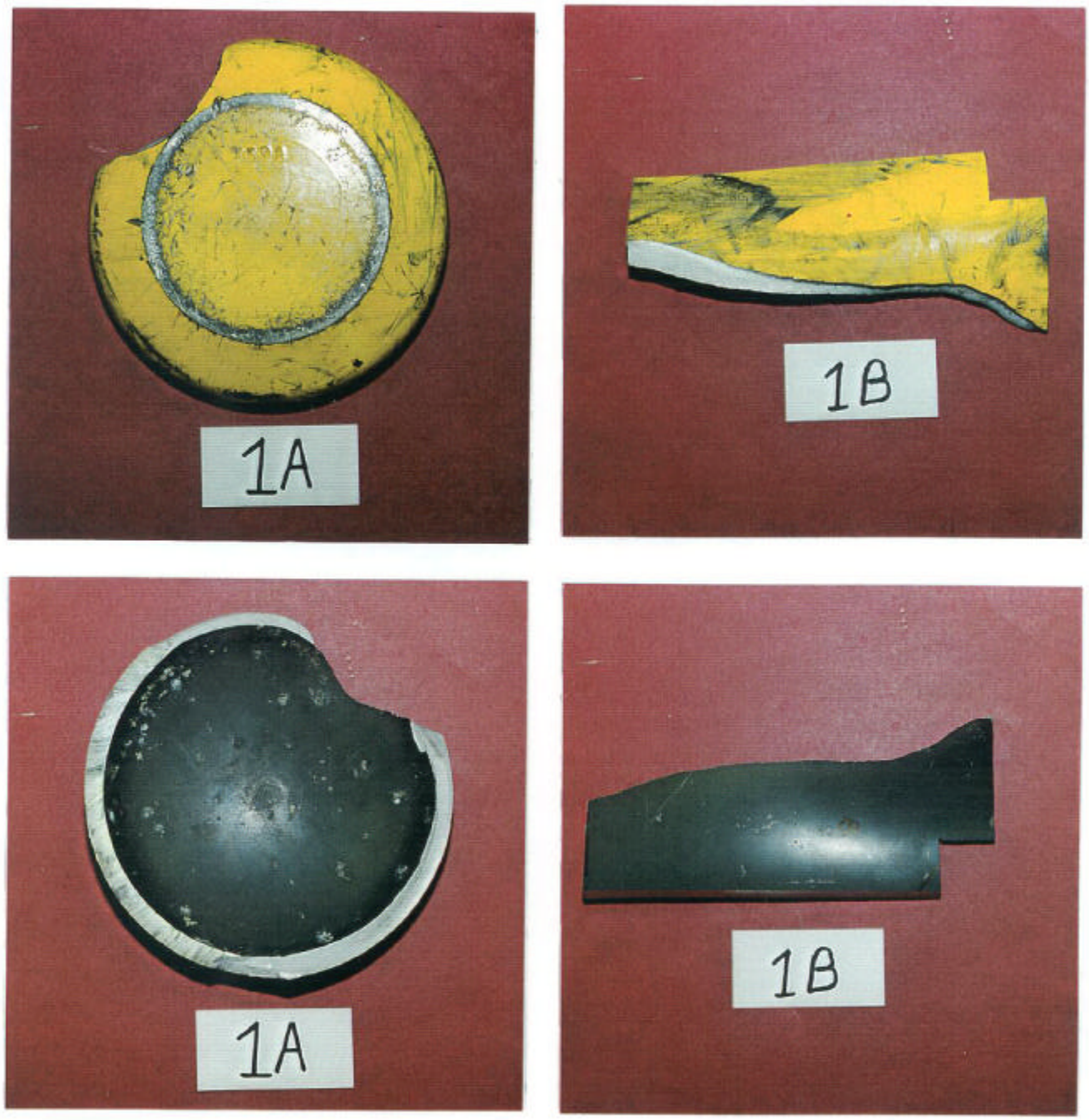


Figure 4. Bottom section (1A) and adjacent lower left side wall fracture edge section (1B) shown in Figure 2.


Figure 5. Tested longitudinal tensile coupon (1C) from lower center section having a 47.7 ksi 0.2% yield strength, 51.7 ksi ultimate tensile strength and 15.5% elongation in 2 in. and remaining lower right fracture edge section (1D) shown in Figure 2.


Figure 6. Upper left fracture edge section (1E) and adjacent failed bend test coupon (1F) shown in Figure 2.

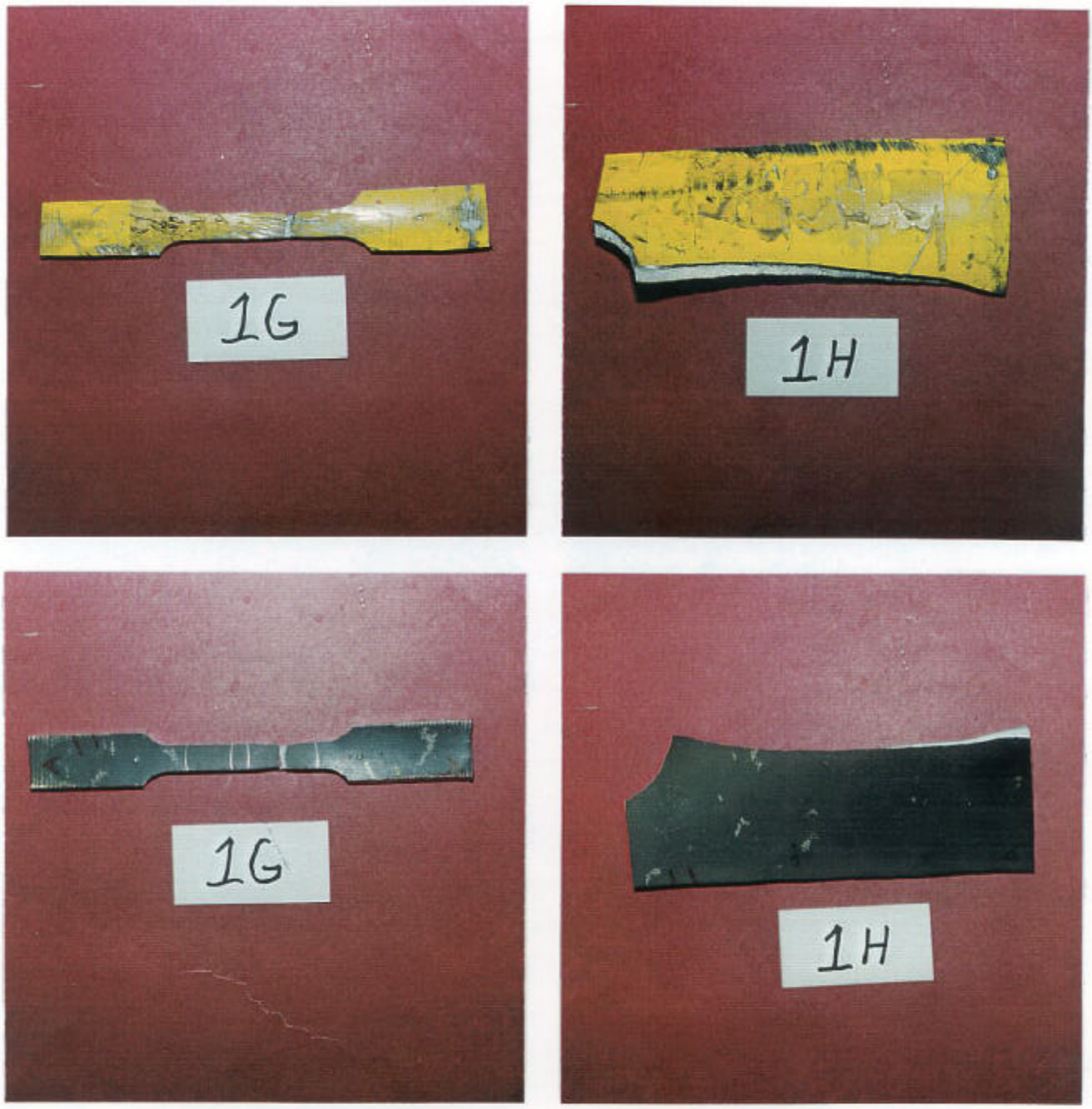


Figure 7. Tested longitudinal tensile coupon (1G) having a 48.0 ksi 0.2% yield strength, 51.5 ksi ultimate tensile strength, and 19.3% elongation in 2.0 in. and remaining upper fracture edge section of (1H) of the cylindrical wall shown in Figure 2.

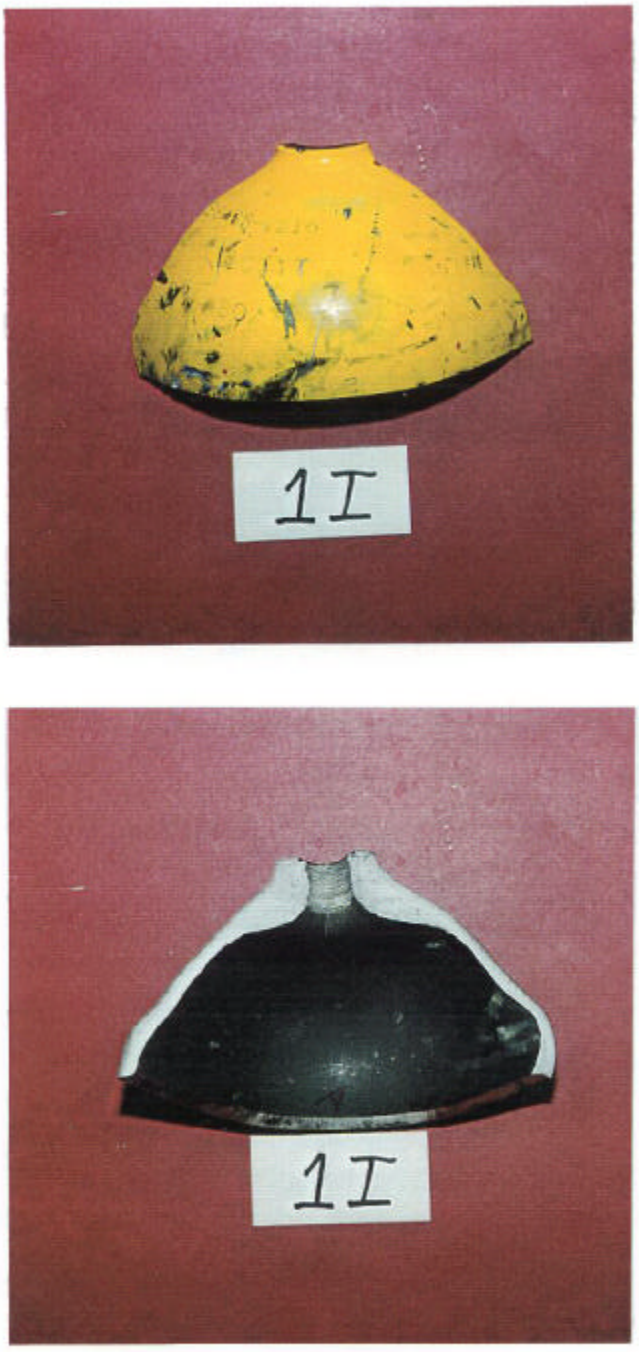


Figure 8. Top section (1I), with fracture faces roughly 120° apart, shown in Figure 2.

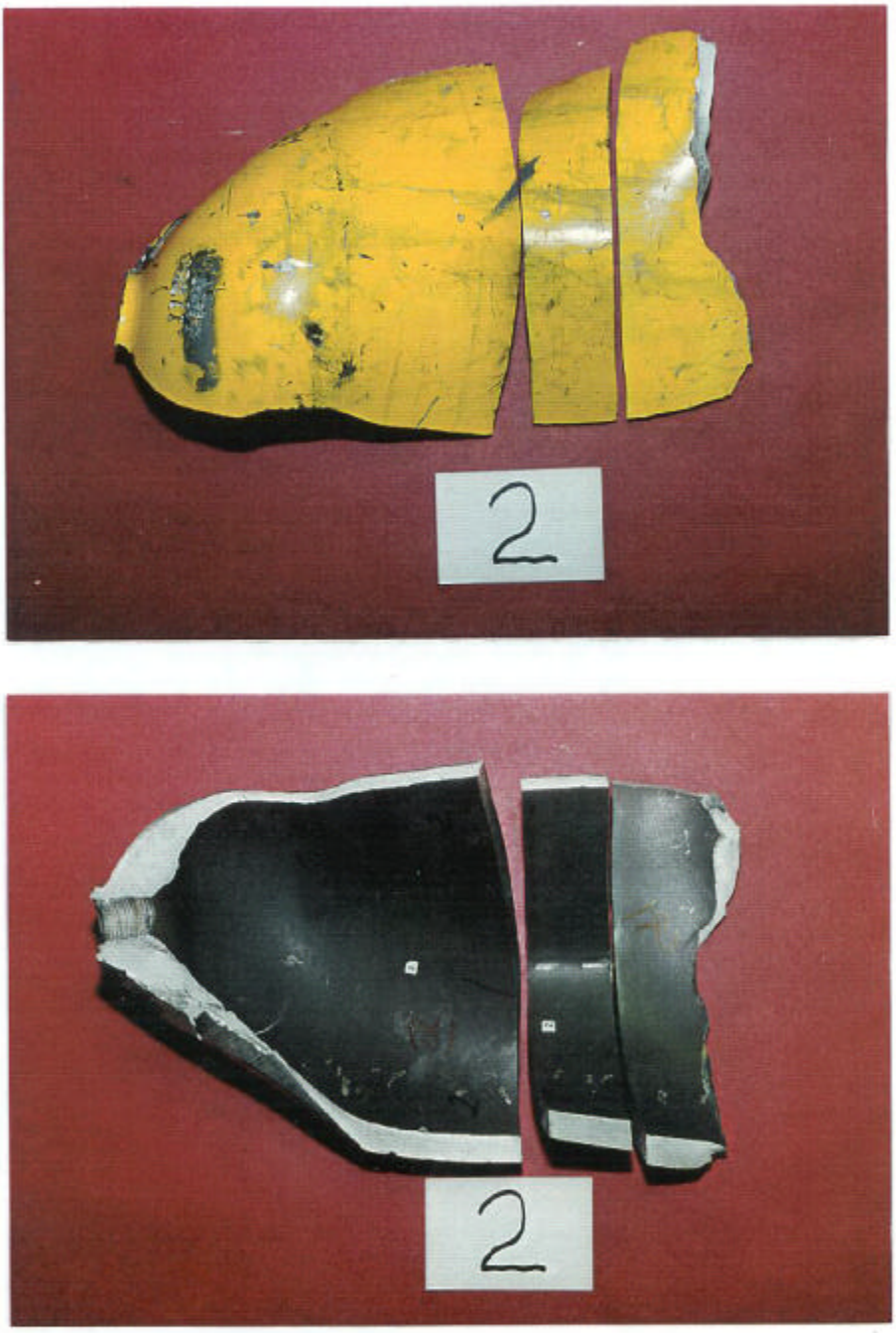


Figure 9. Fracture piece (2), with transverse section previously tested as a bend test coupon that failed during testing, shown in Figure 1.

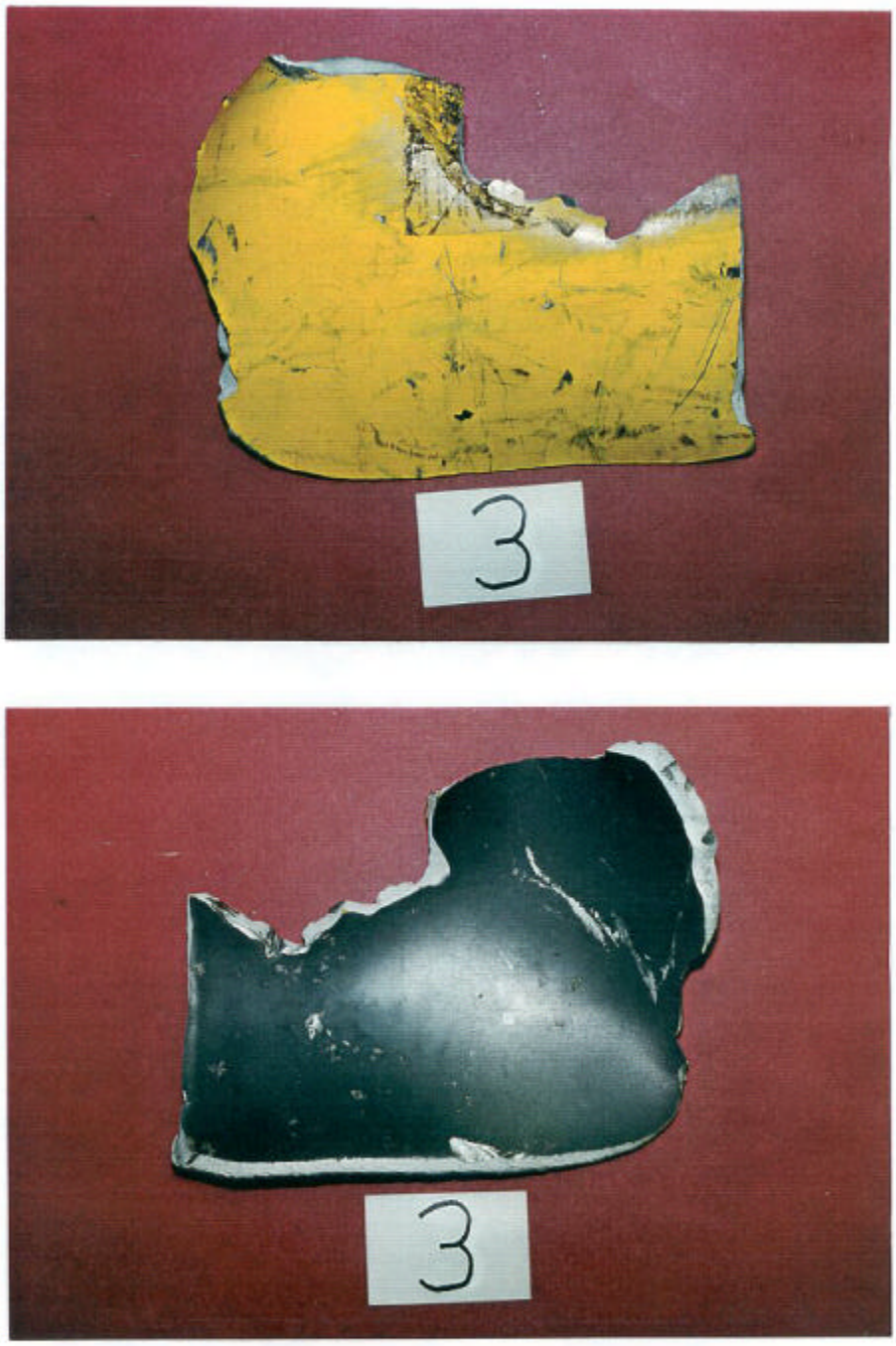


Figure 10. Fracture piece (3), adjacent to bottom of cylinder, shown in Figure 1.

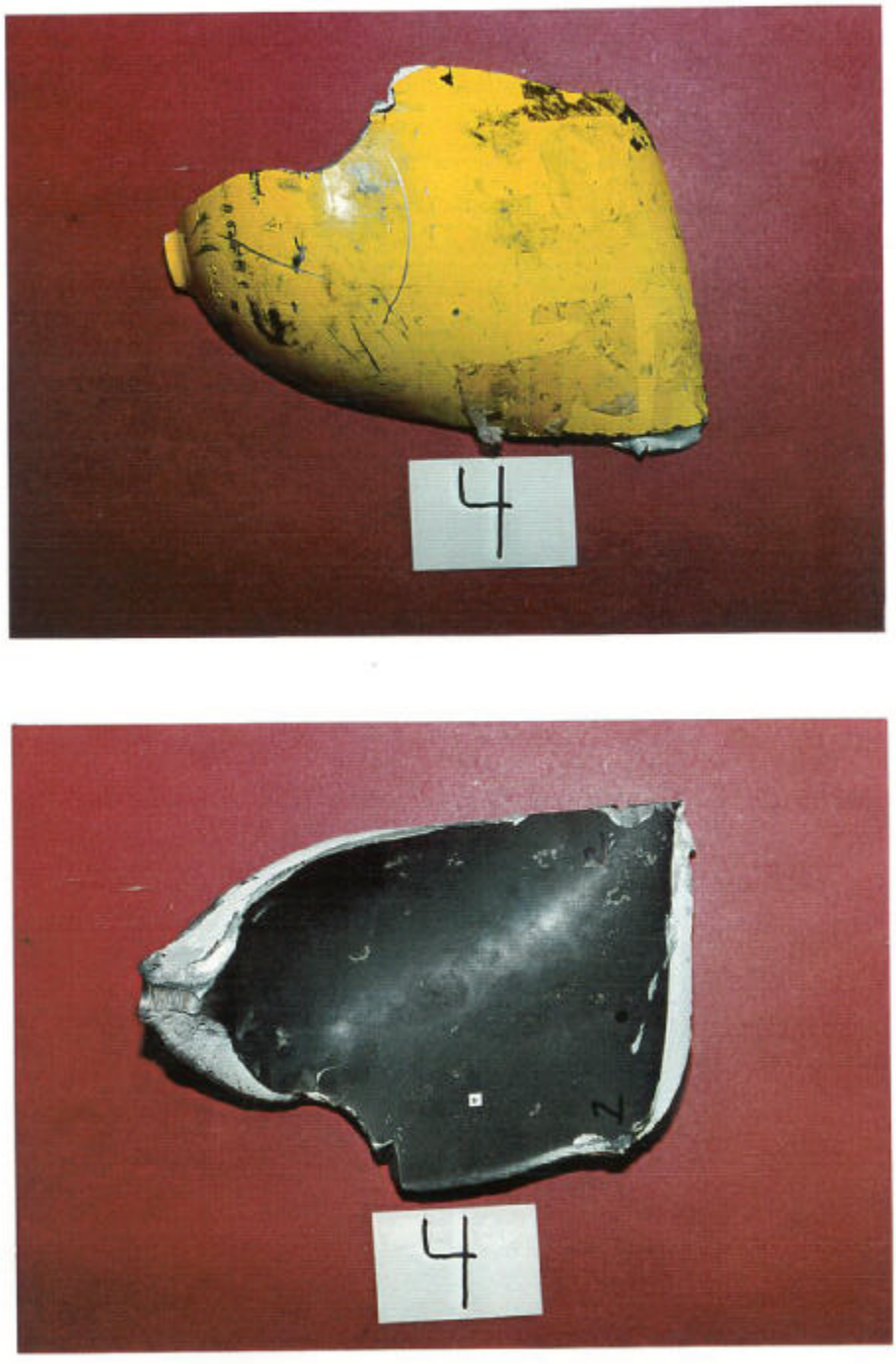


Figure 11. Fracture piece (4), from top of cylinder shown in Figure 1.


Figure 12. Fracture piece (5) from lower half of cylinder shown in Figure 1.

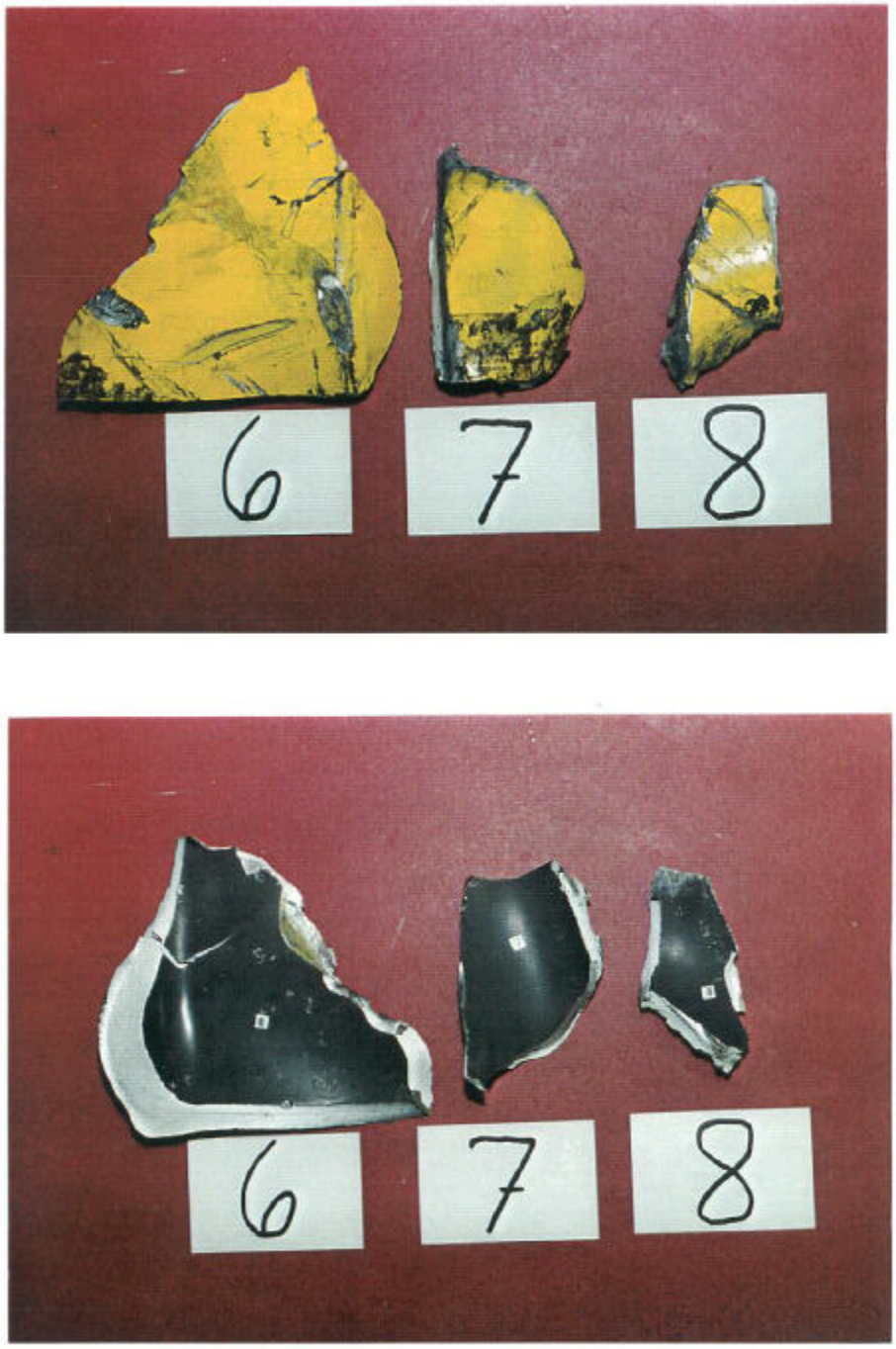


Figure 13. Fracture pieces (6), (7), and (8) from side-wall area adjacent to bottom of cylinder shown in Figure 1.


Figure 14. Fracture fragments (9) through (18) whose location was not identifiable due to small size and fracture surface damage.

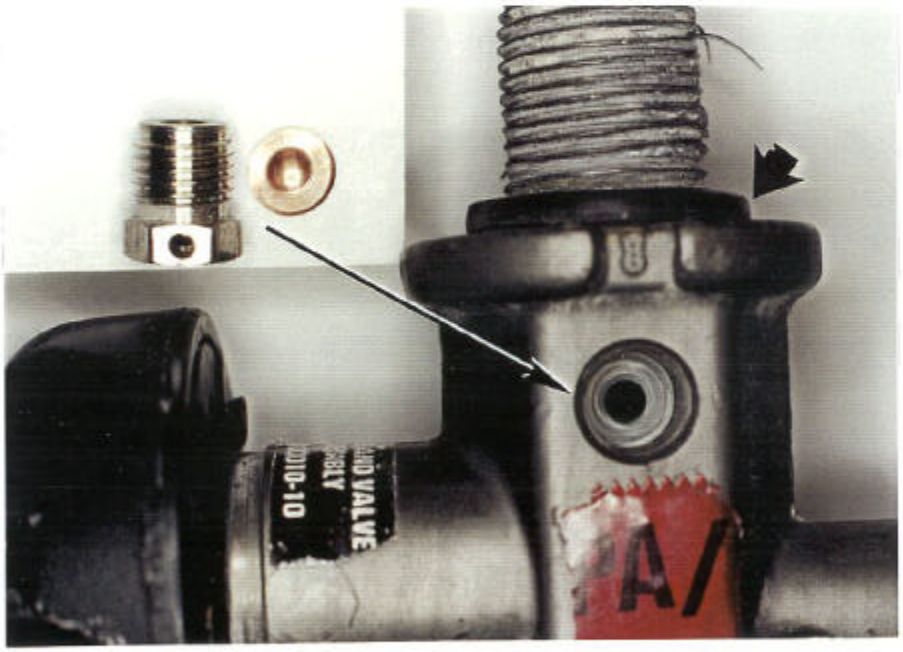

Figure 15. Valve from exploded cylinder showing "O" ring seal (arrow), deformed and several sheared threads, deformed copper rupture disk and retainer. Note white corrosion product on threads.




Figure 16.

Identification markings from heavy wall area at top of cylinder. Note ball peened area below the 11-89 Retester Identification Number.


Figure 17. Identification mark(s) on the bottom of the cylinder. The significance of letter "A" following "X59", the Lot Code, and the unrecognized symbol in the lower photograph is not known at this time.

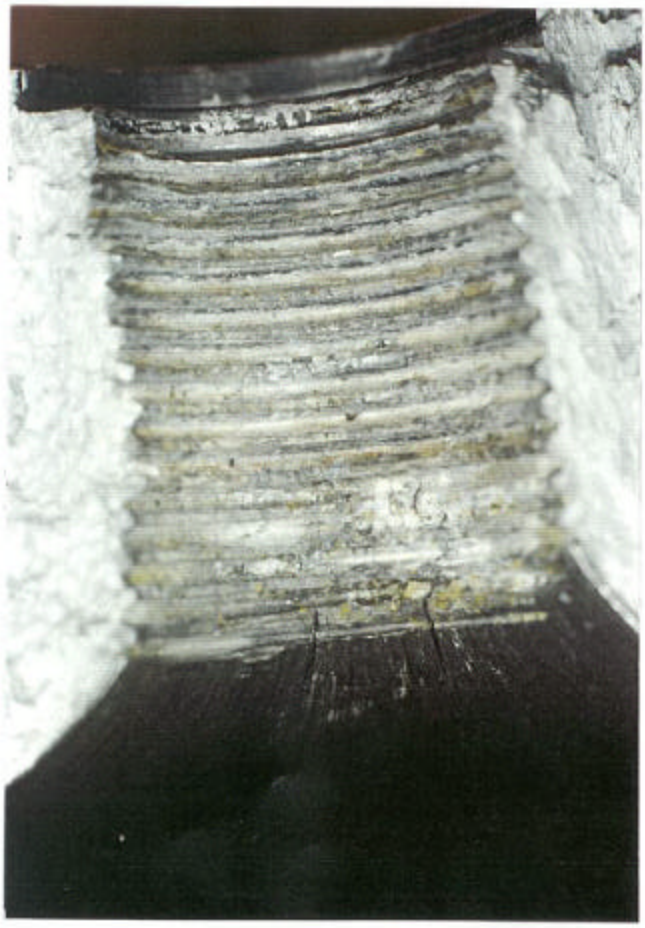

Figure 18.

Enlarged views of the internal thread for receiving the valve revealing the as-received condition of fracture piece (2) at top left, fracture piece (4) at top right, and fracture piece (1I) at lower left. Note the additional cracks in the interior neck area and the more corroded area of the fourth thread from the bottom.


Figure 19. Fracture specimen from an exemplar cylinder (S/N 240868) from Lot Code X59 that was over-pressurized in excess to the design burst pressure.

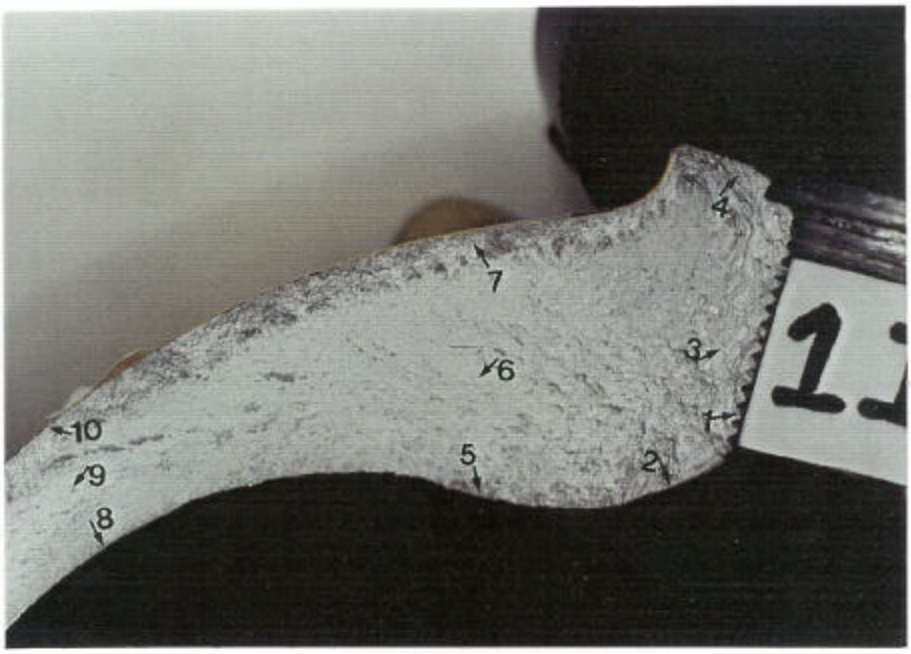


Figure 20. A macro view of the fracture surface #1 which was examined to characterize the fracture features. Areas indicated by arrowed numbers were examined at higher magnifications under the SEM.

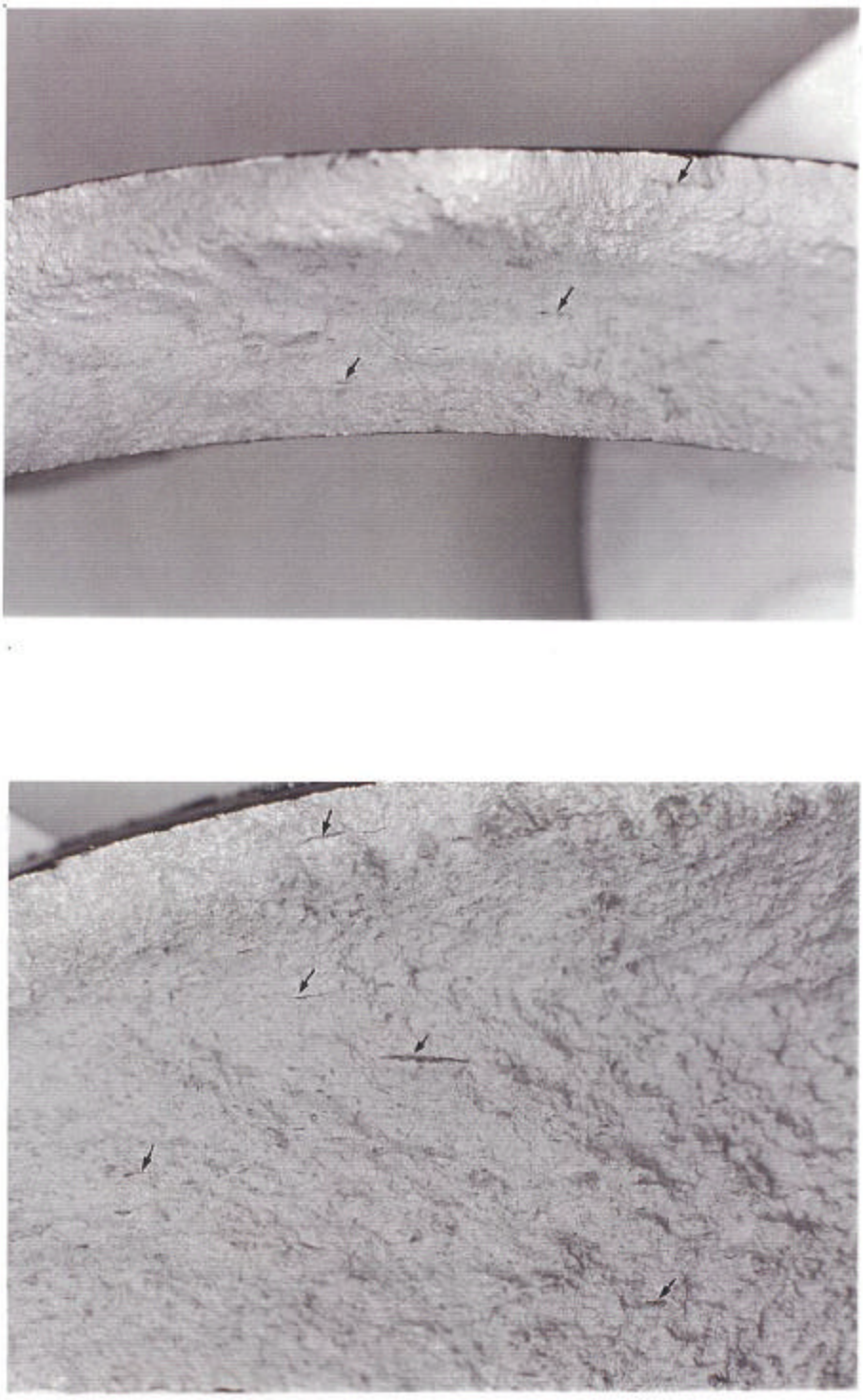

Figure 21. Enlarged photographs of the fracture surface show a large population of dark streaks.

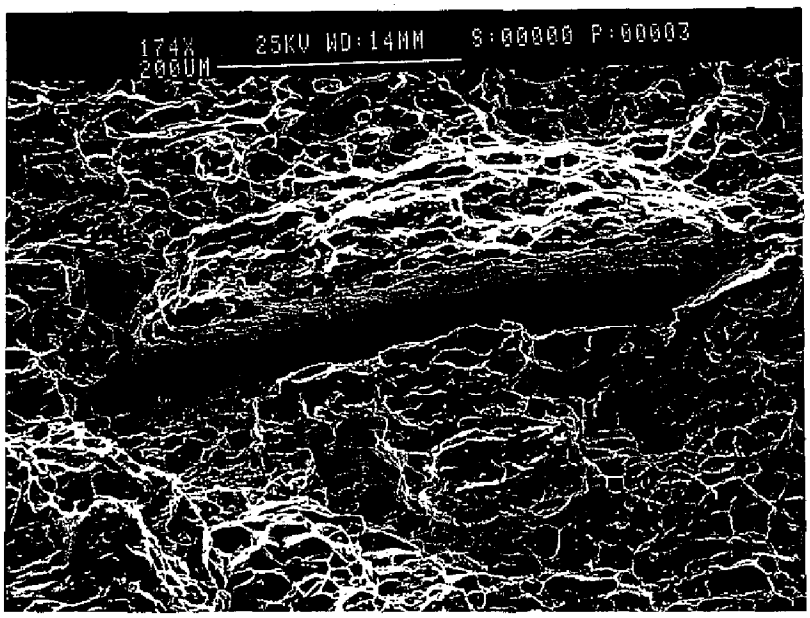


Figure 22. SEM micrograph shows a high magnification view of dark streaks indicated in figure 21. It appears like voids having textured/rough surfaces; X174.

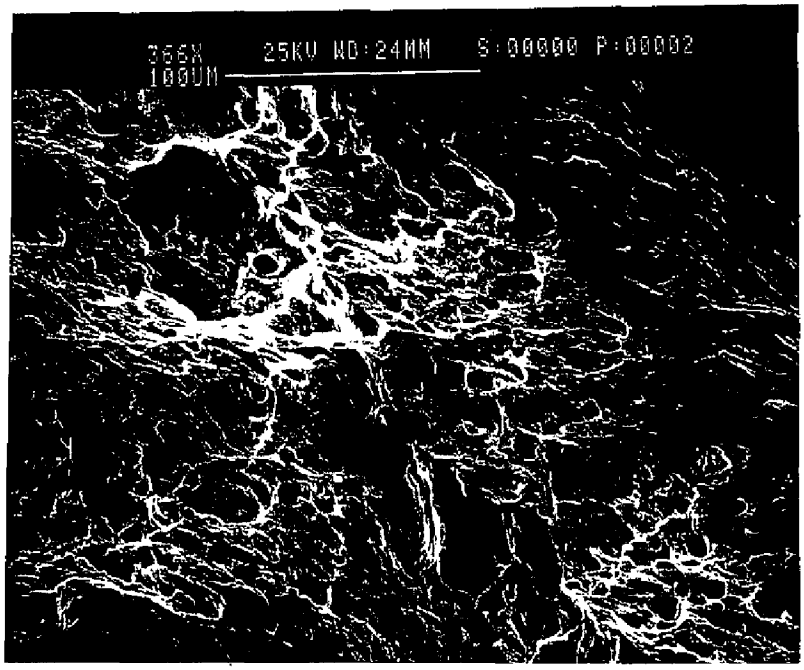


Figure 23. SEM fractograph, from location #1 in Figure 20, exhibits fracture initiating at threads. The failure occurred in tearing mode due to overload, indicated by elongated dimples; X366.

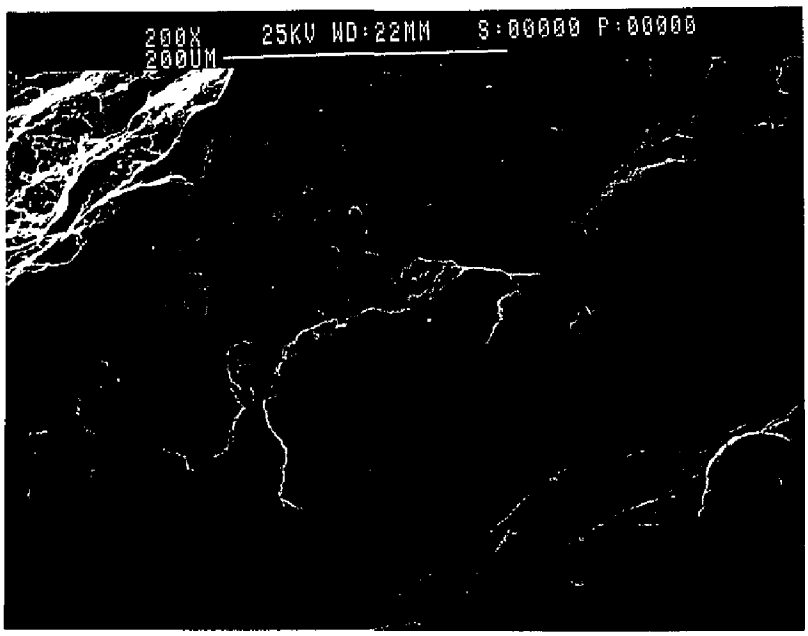


Figure 24. Fracture appearance at location #2 is mostly featureless. Some evidence of overload dimples is also indicated; X200.

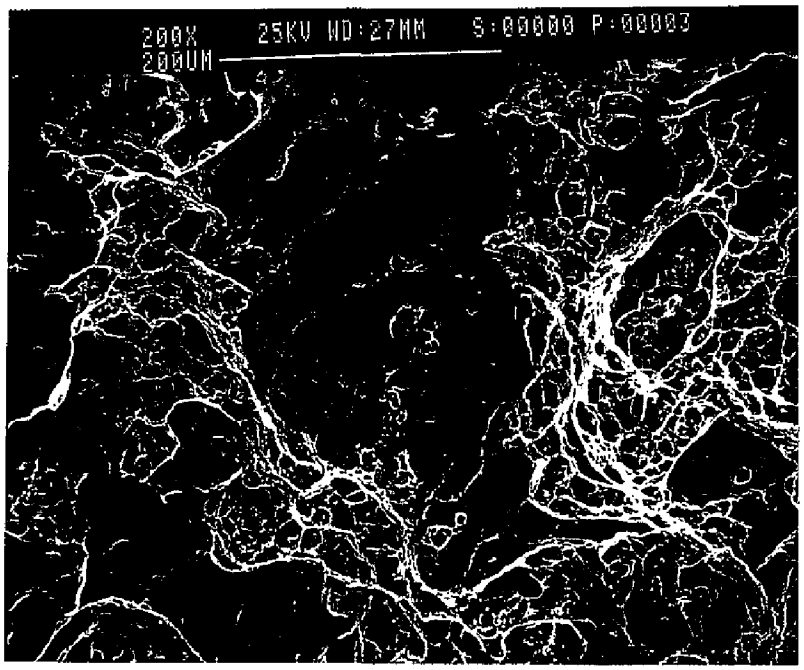


Figure 25. Fractograph from location #3 shows similar features as in Figure 24; X200.

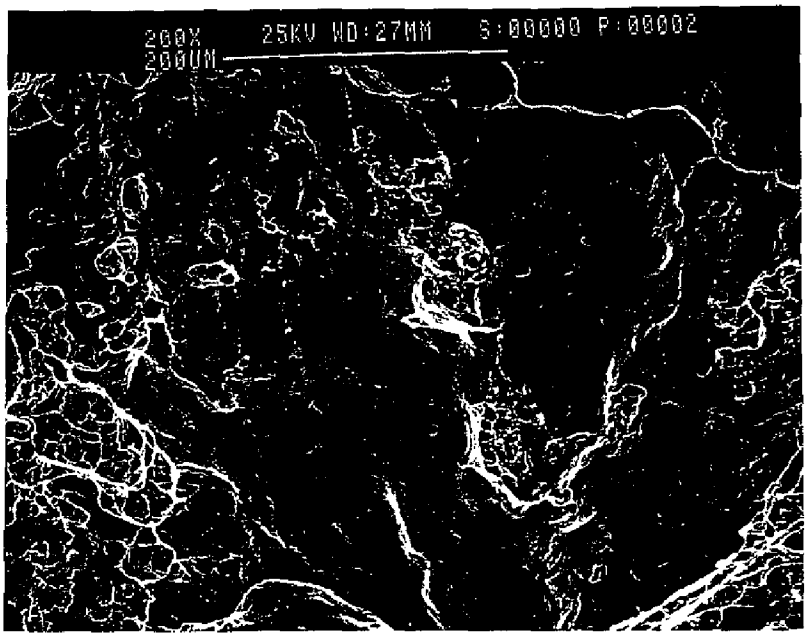


Figure 26. Fractograph from location #4 exhibits similar features as in Figure 24; X200.

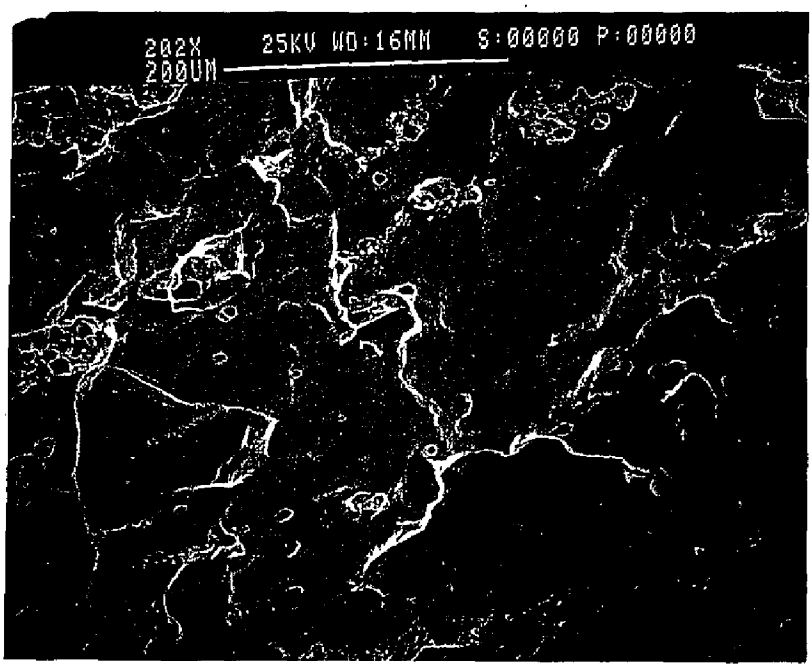


Figure 27. Fractograph from location #5 shows similar features as in Figure 24. The fracture initiated along the metal fold formed on the inside surface during manufacturing process; X202.

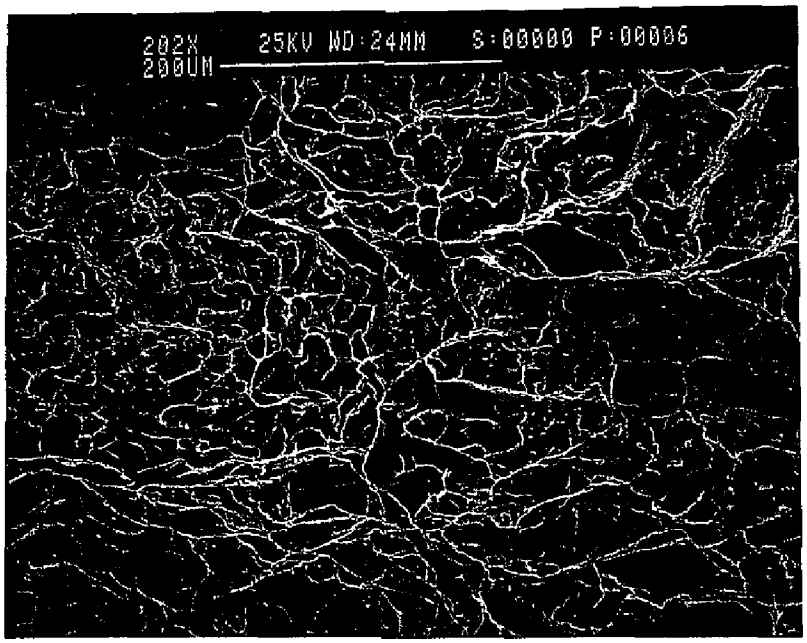


Figure 28. Fractograph from location #6 shows failure due to dimpled (overload) fracture; X202.

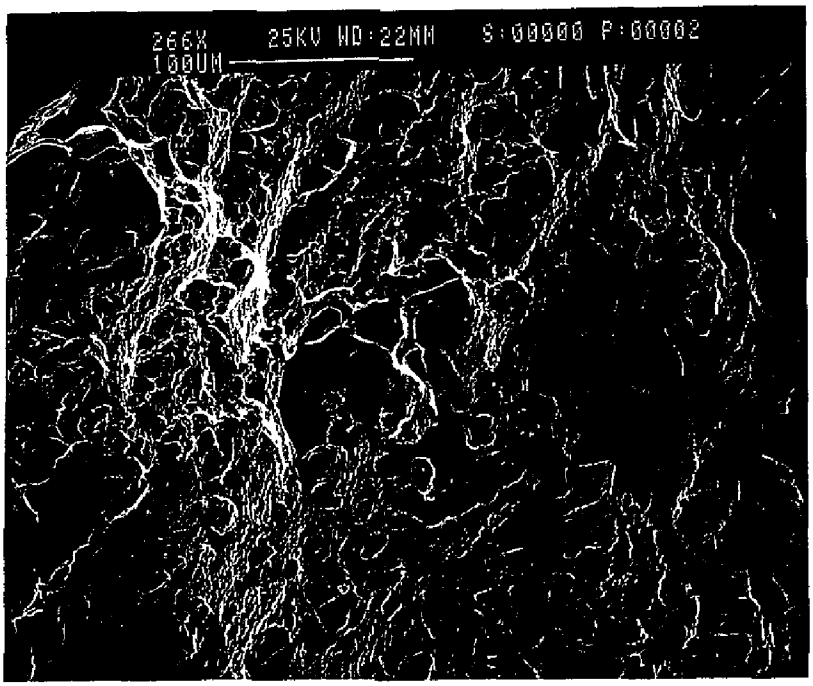


Figure 29. Fractograph from location #7 showing similar features as in Figure 28; X266.

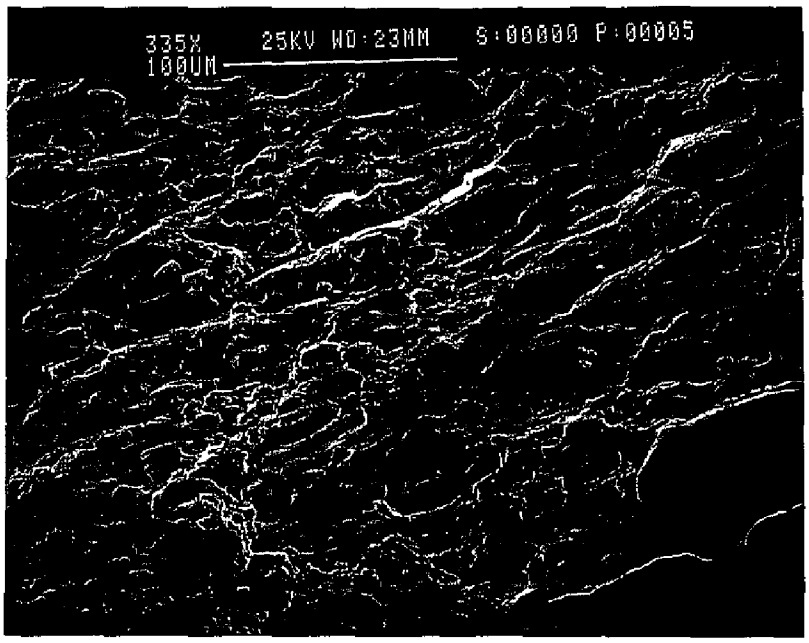


Figure 30. Fractograph from location #8 showing failure due to overload. Some indications of grain boundary failure are evident; X335.

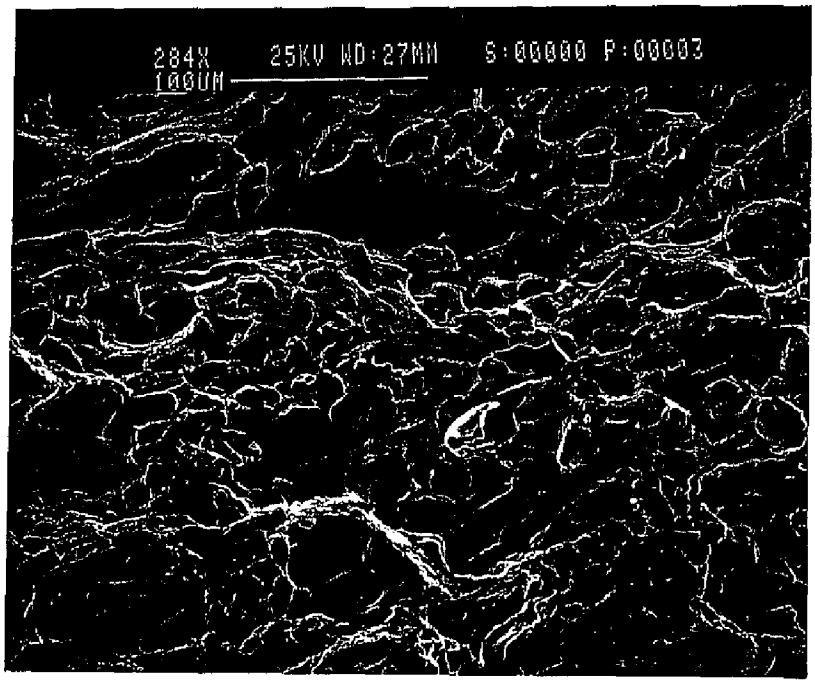


Figure 31. Fractograph from location #9 exhibits similar features as in Figure 30 showing a mixed mode of failure; X284.

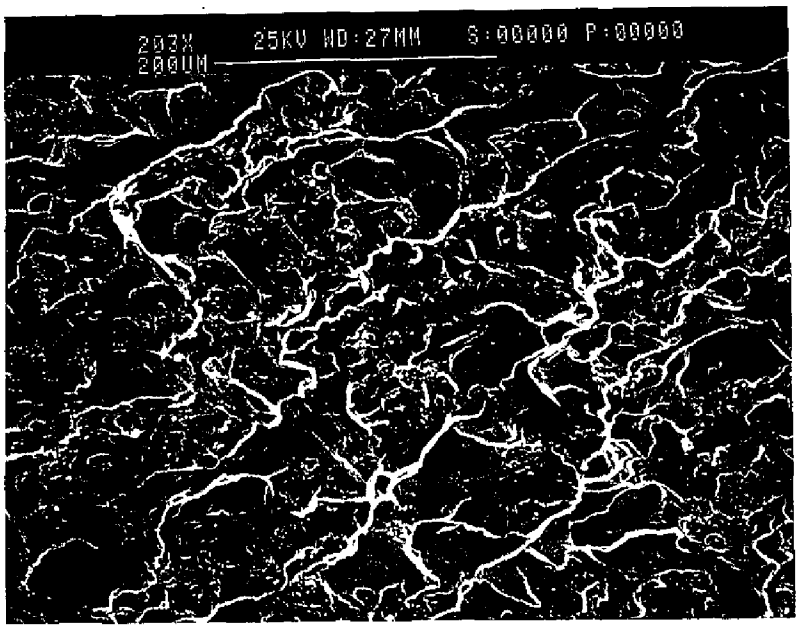


Figure 32. Fractograph from location #10 shows failure due shear overload; X203.

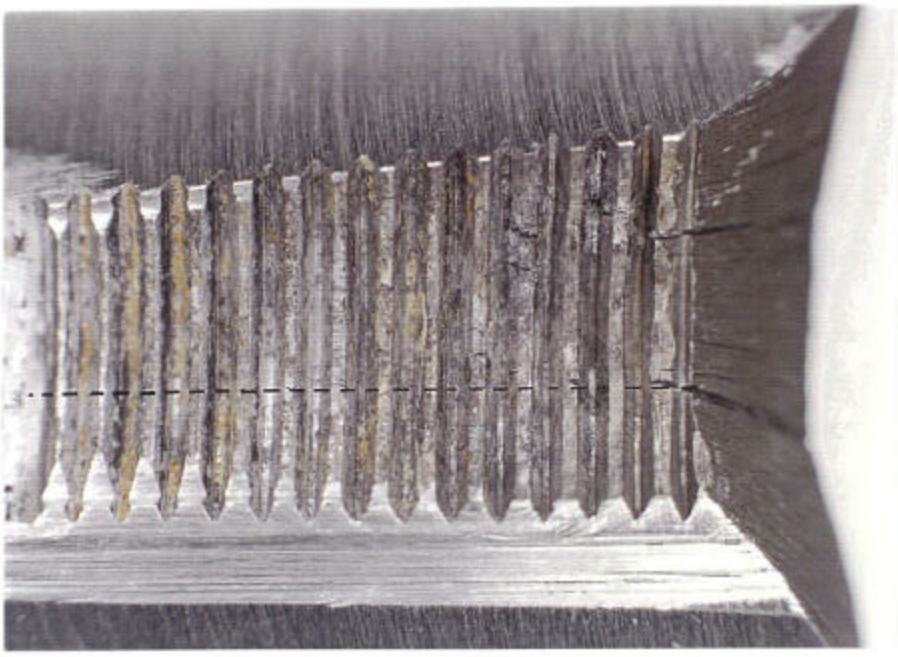

a.

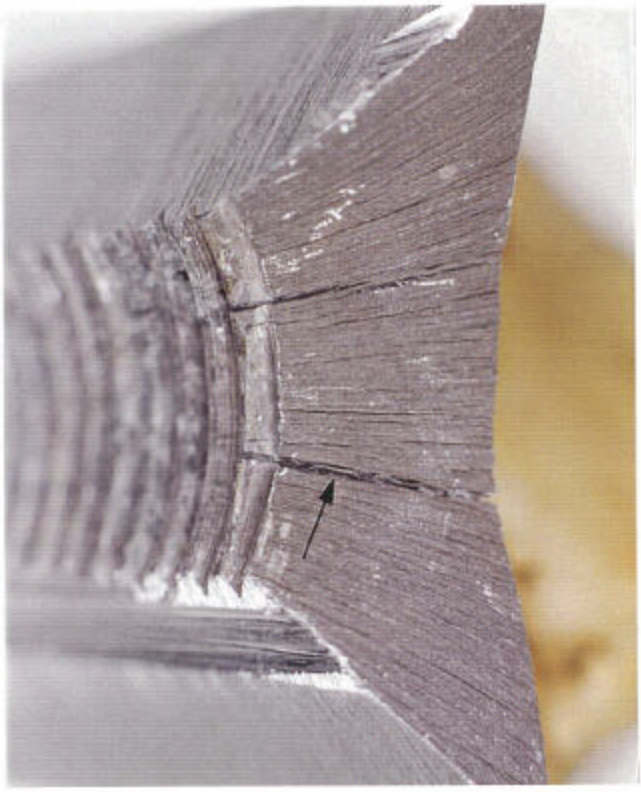

b.

Figure 33. Photographs of an area from the neck region showing the threaded zone (a) and the adjacent internal surface (b). Note the crack-like features in both photos. The crack indicated by arrow was opened for detailed examination.

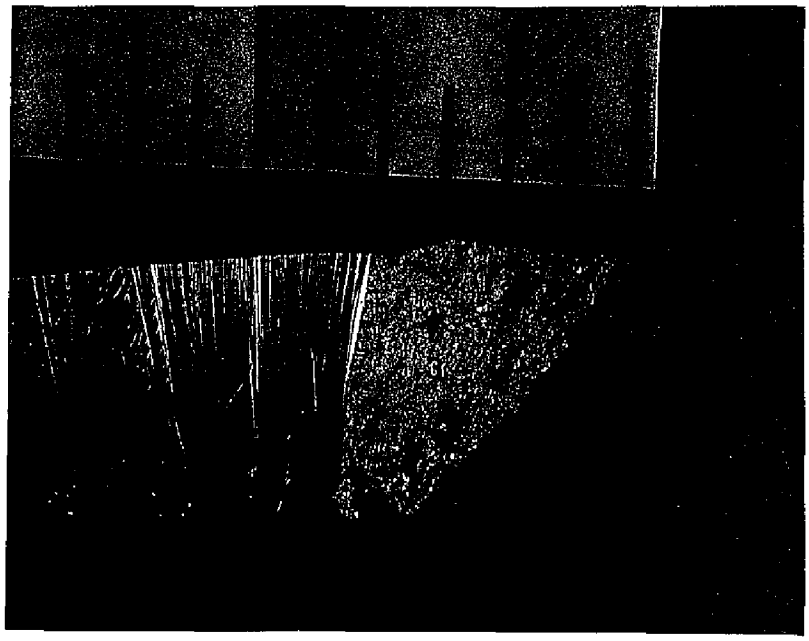

Figure 34. An enlarged view of the lab-created fracture surface. Locations indicated by arrowed numbers were examined at higher magnifications; X6.

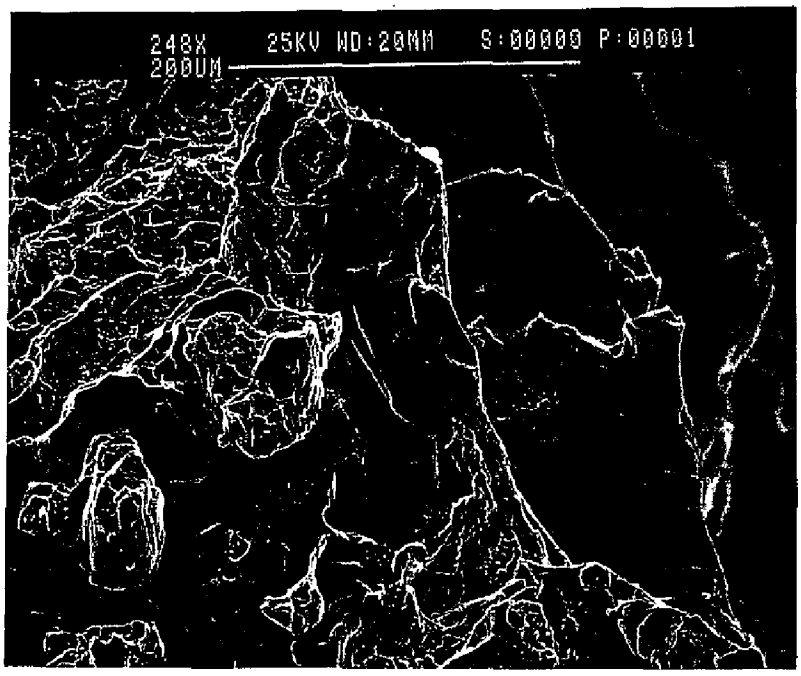


Figure 35. Fractograph, from location #1 in Figure 34, exhibits featureless facets as indicated in Figures 24-27. It also shows some area having dimpled rupture; X248.

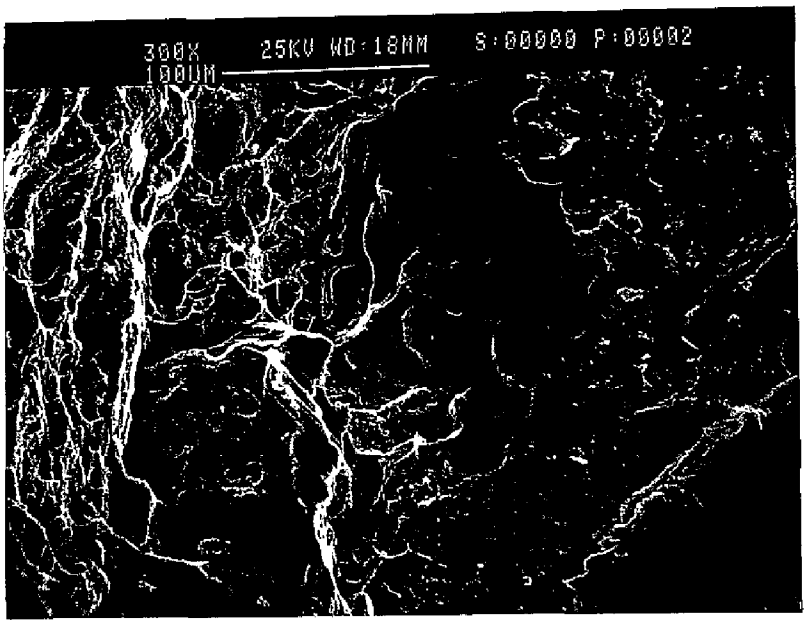


Figure 36. It shows similar features as in Figure 35; X248.

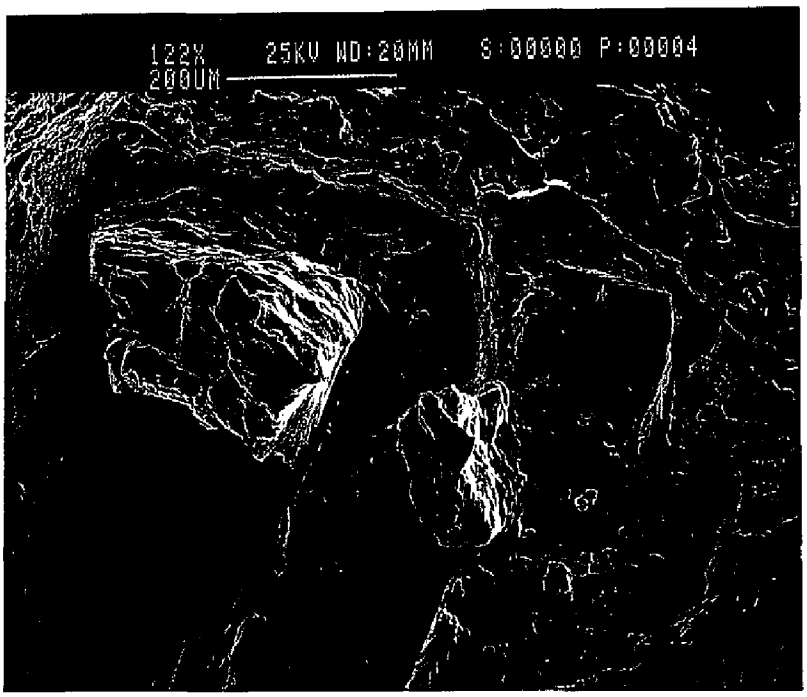


Figure 37. Fractograph exhibits featureless facets and some dimpled rupture. The particle-like object (arrow) appears to be a chunk of dross. X122.

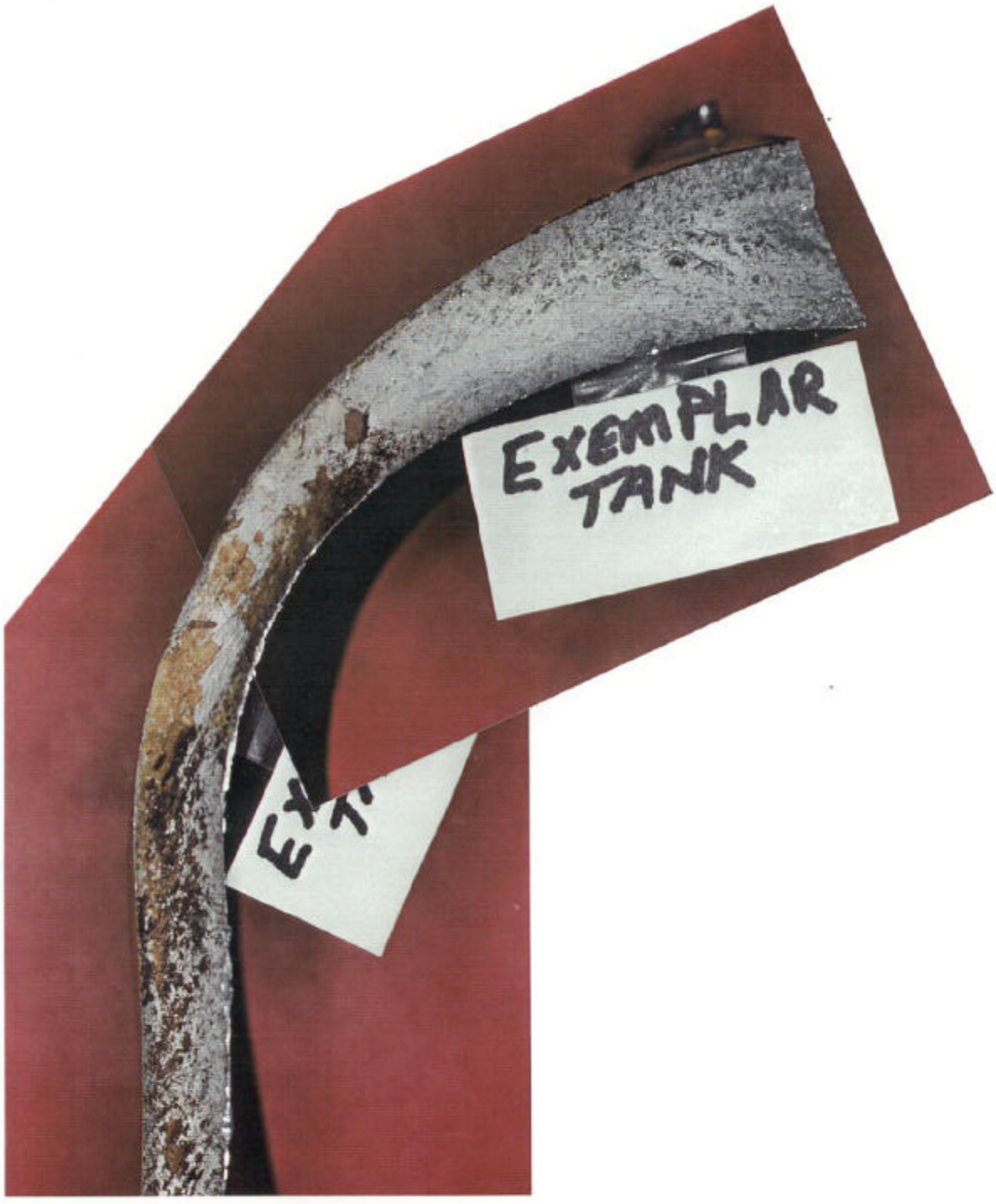


Figure 38. As-received view of the exemplar fracture surface.

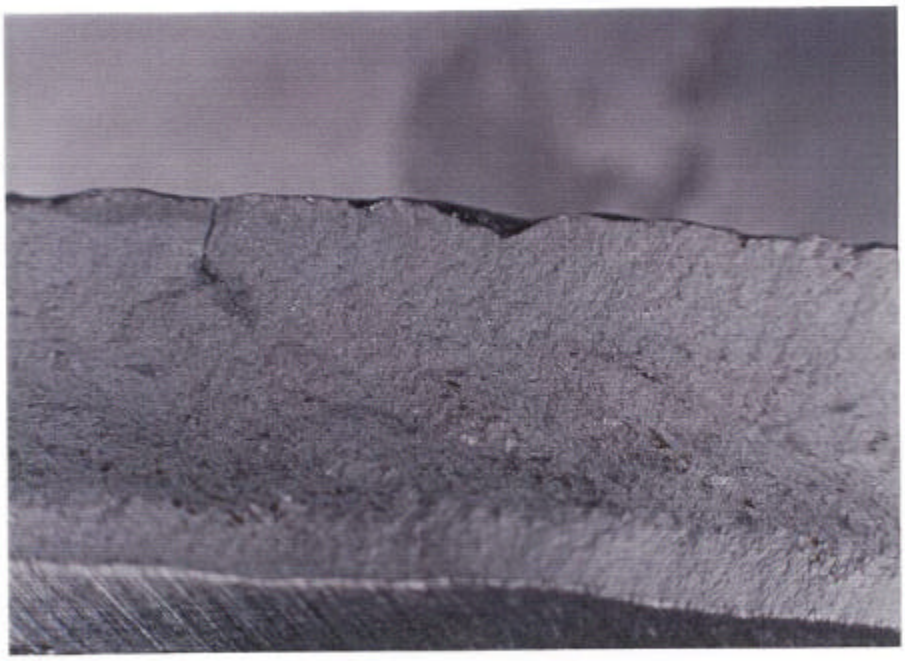

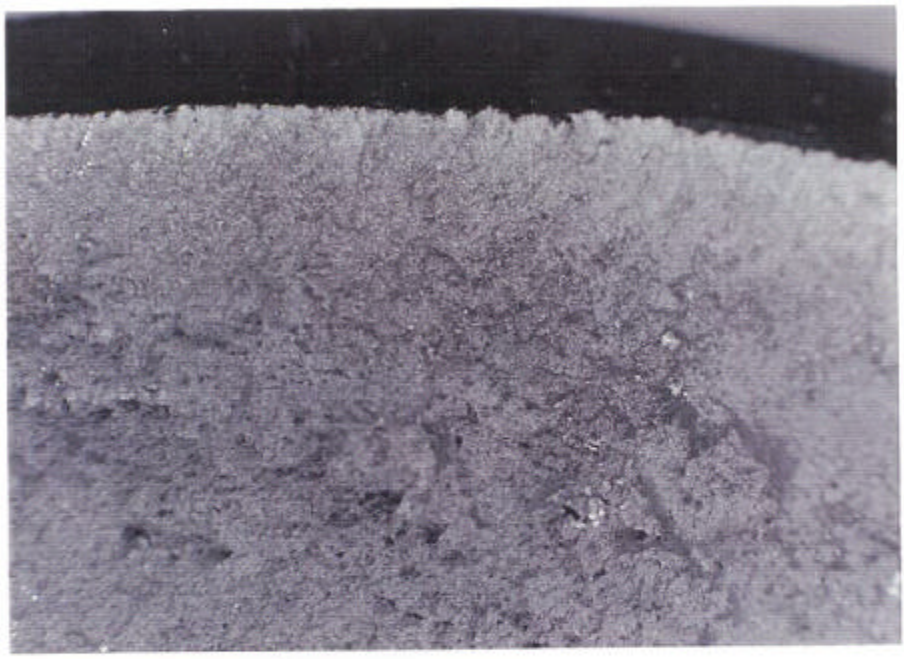

Figure 39. Enlarged views of the fracture surface does not show the presence of dross and voids. Compare this Figure to Figure 21.

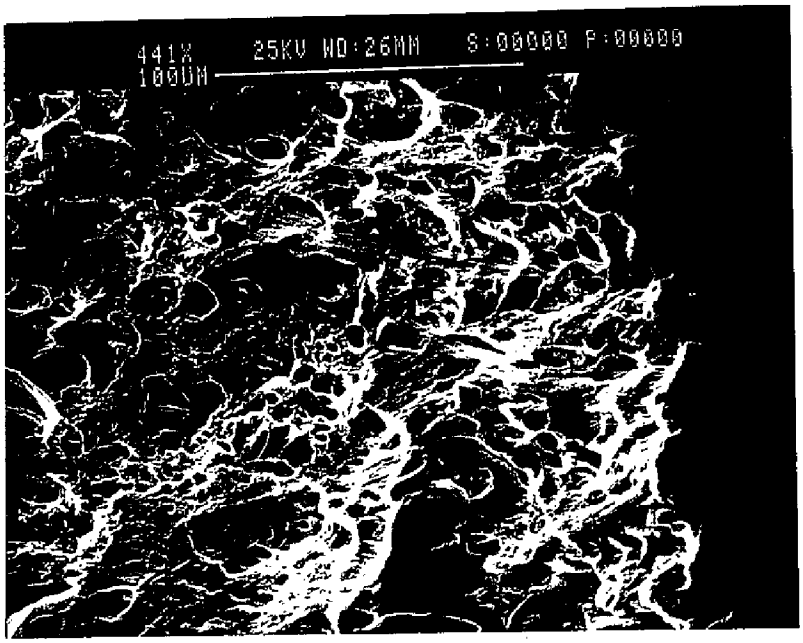


a;X441

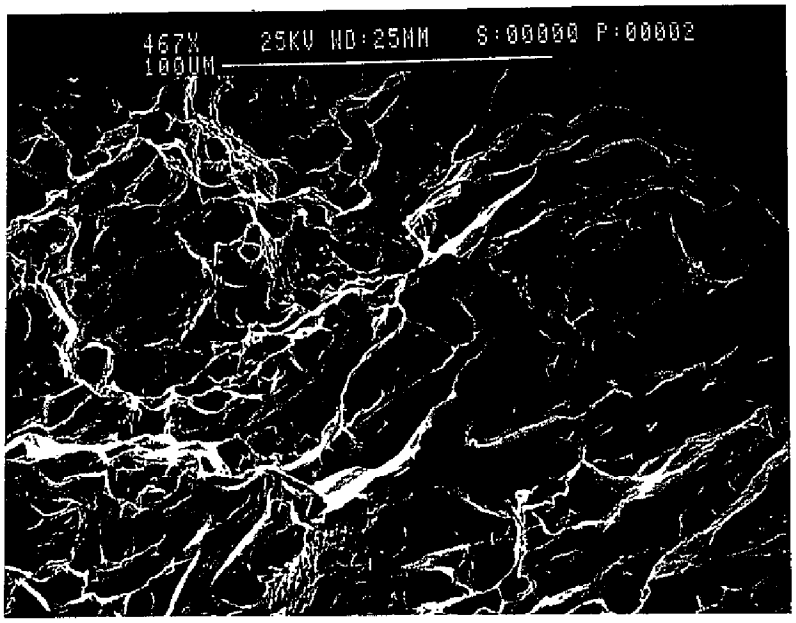


b;X467

Figure 40. SEM fractograph shows initiation of the failure occurring by overload tearing near the neck on the inside surface (a); a mixed mode failure consisting of dimpled rupture and intergranular fracture was observed in the region remote from the initiation zone (b). Compare these micrographs to Figures 23 and 30.

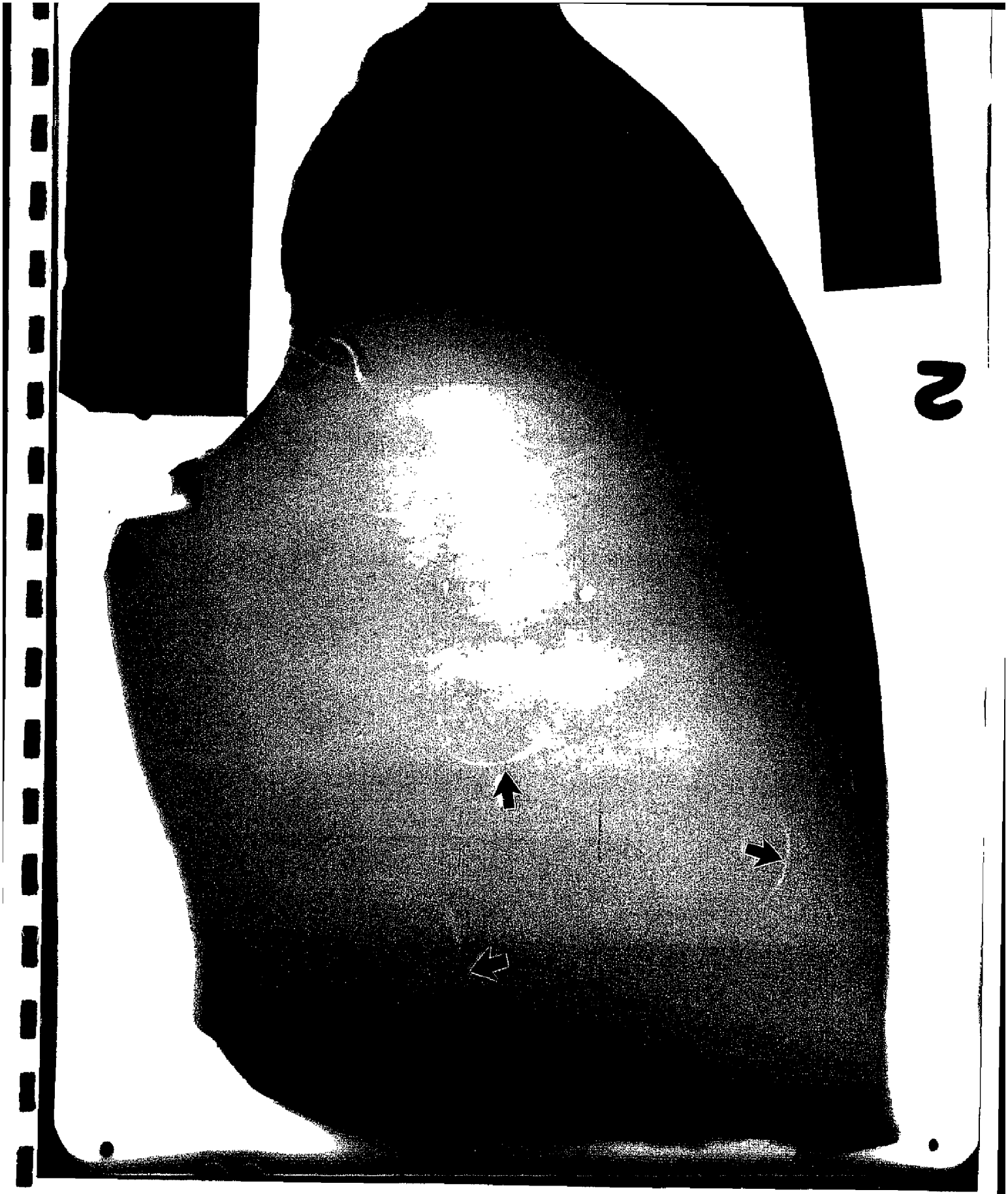

Figure 41. Positive print of an X-ray radiograph of fracture piece (4) showing several indications (arrows) not attributable to surface damage.

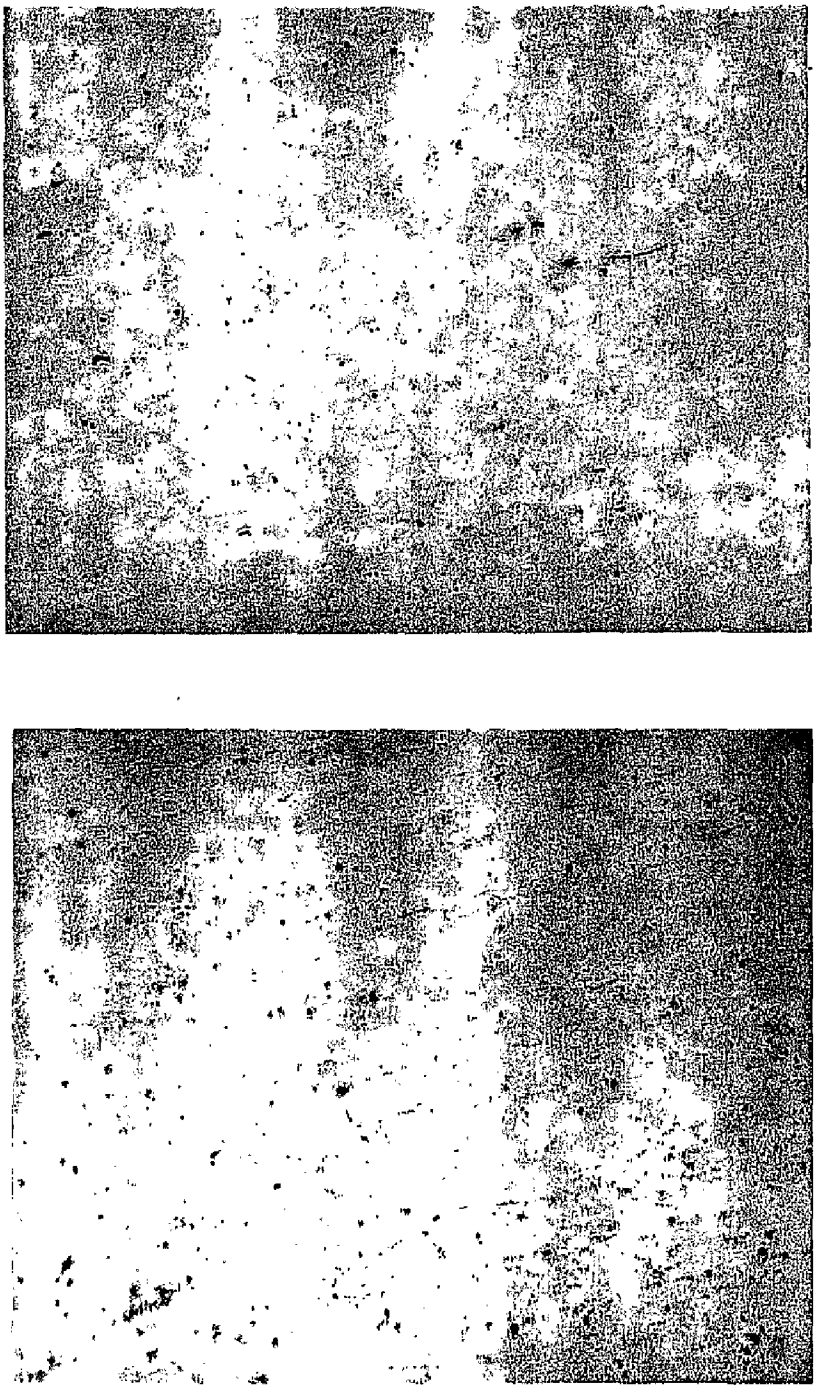

Figure 42. As-polished transverse sections, from an X-ray radiograph indication in fracture piece (4) (top) and from exemplar fracture sample (bottom) showing relatively higher and more elongated inclusion content in the radiographic indication, X50.

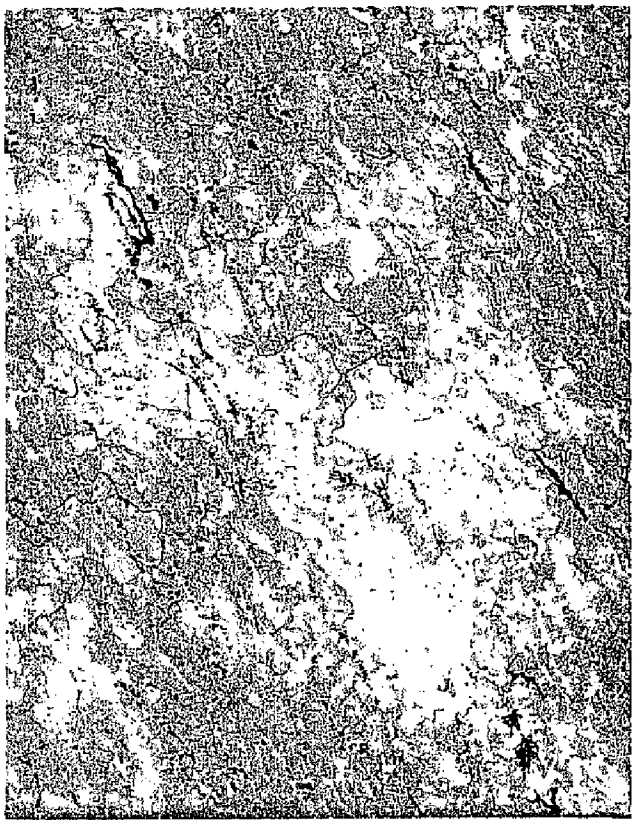

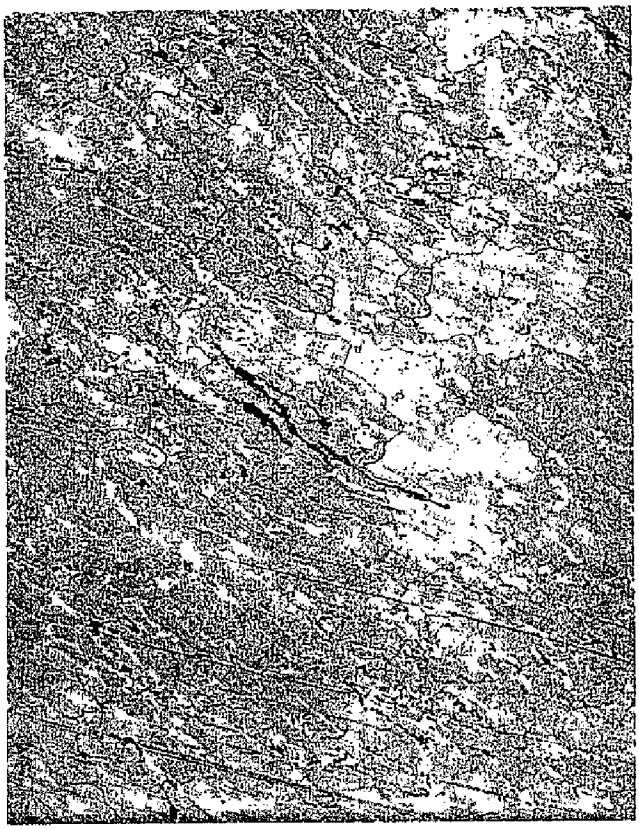

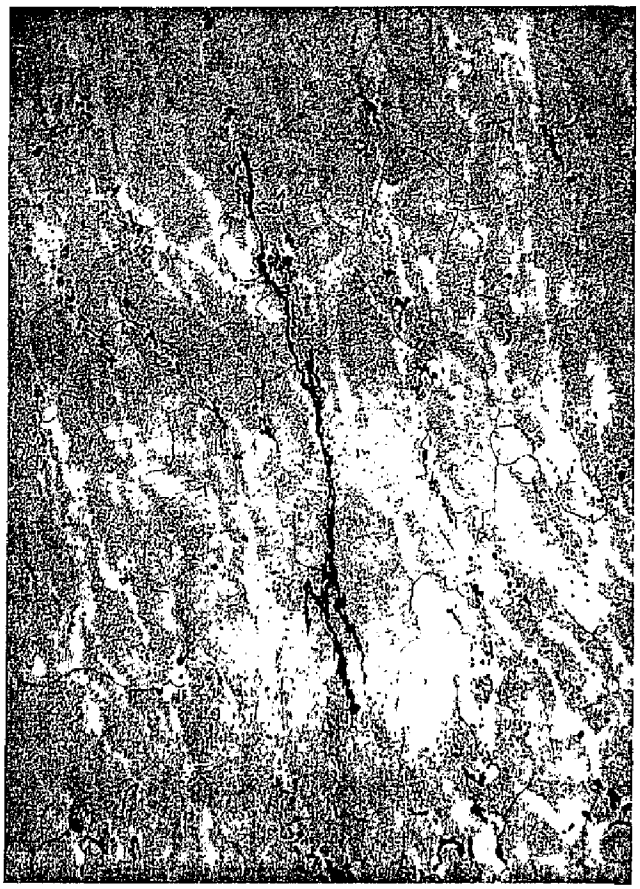

Figure 43.

Radial plane approximately 1/8 inch from fracture common to fracture pieces (1I) and (4) in the heavy wall area exhibiting several forms of entrapped dross, 1% NaOH etchant, X50.

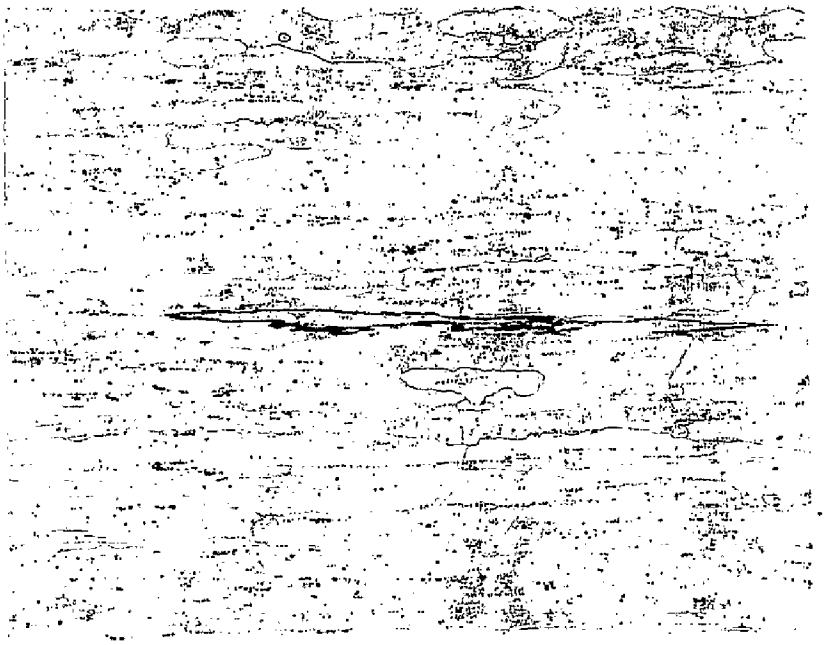

Figure 44. Dross entrapment in longitudinal section of threaded heavy wall area, 1% NaOH etchant, X50.

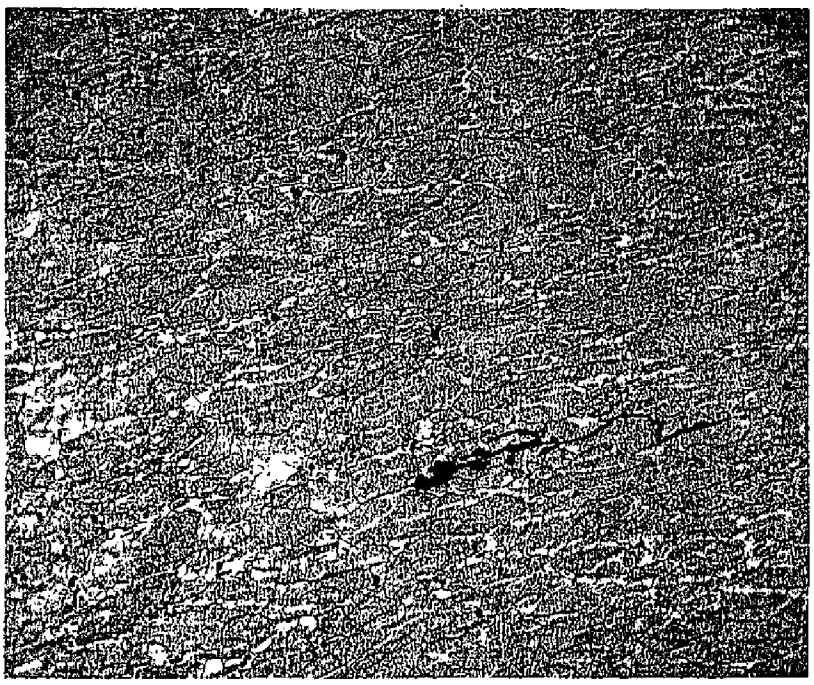

Figure 45. Dross entrapment in a radial section from the bottom of the fragmented cylinder, 1% NaOH etchant, X100.

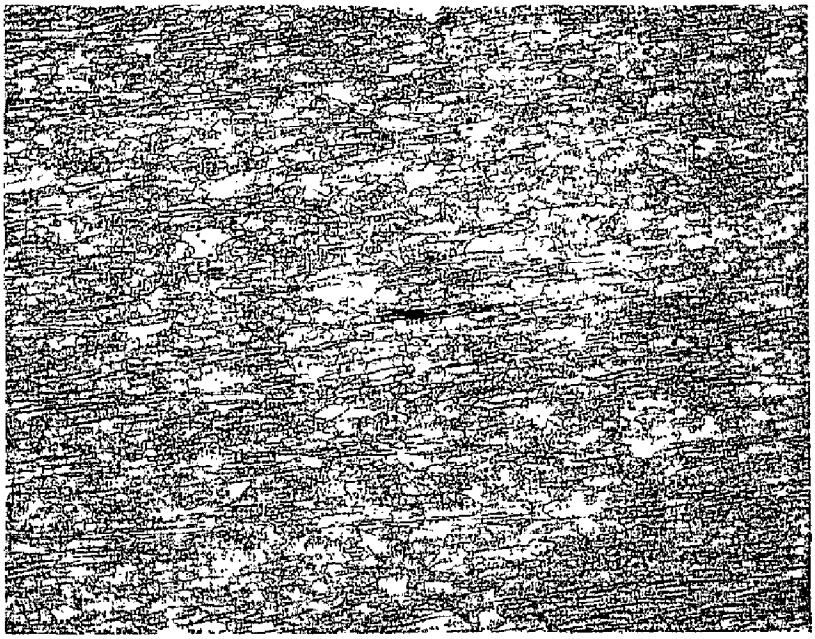

Figure 46. Dross entrapment in a transverse section from fracture piece (2), 1% NaOH etchant, X50.

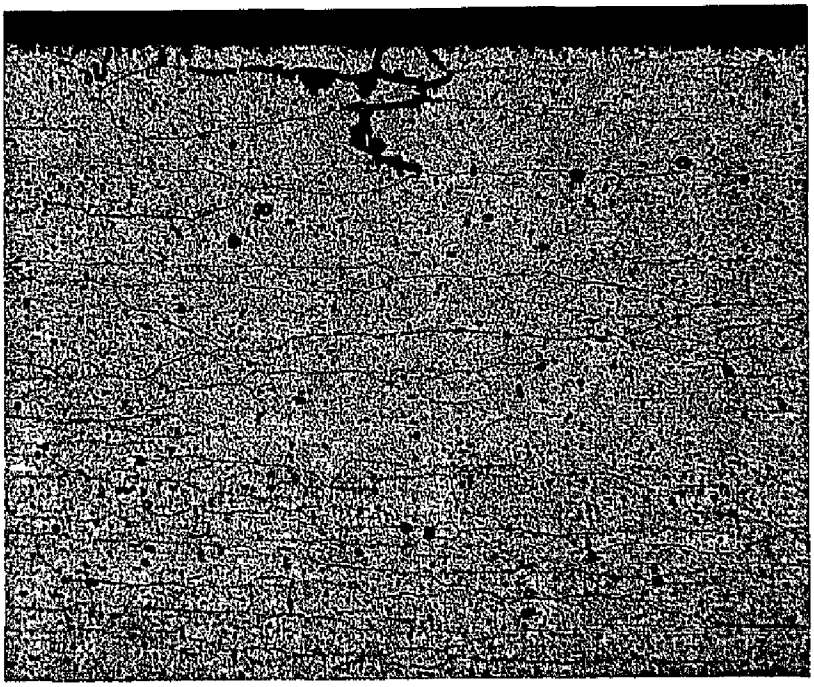

Figure 47. Grain boundary corrosion observed on interior surface in a radial section through the angular transition area of bottom to side wall, 1% NaOH etchant X200.

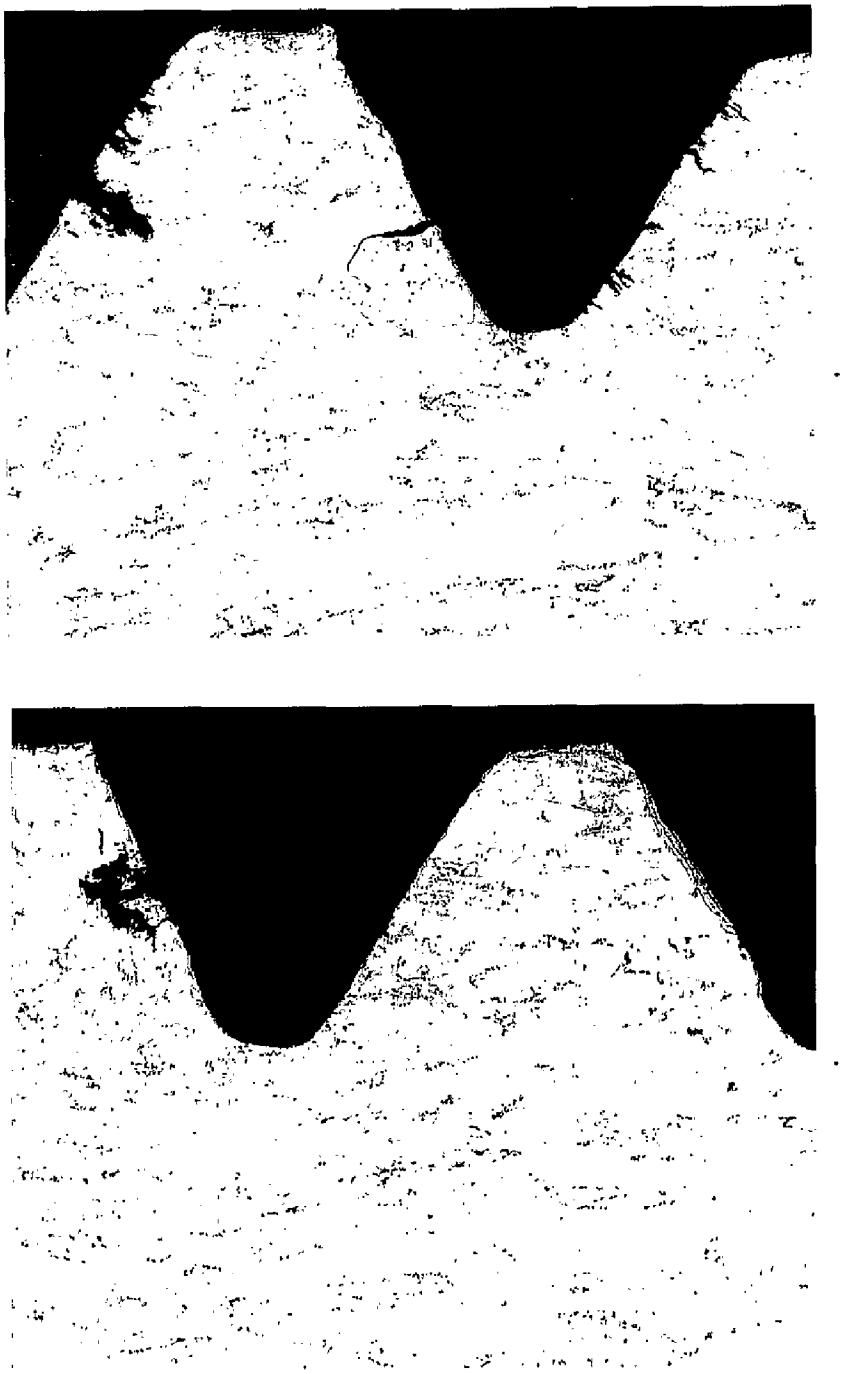

Figure 48. Radial section through top area of threads, exhibiting corrosion attack normal to thread surface and along grain boundaries, 1% NaOH etchant, X50.

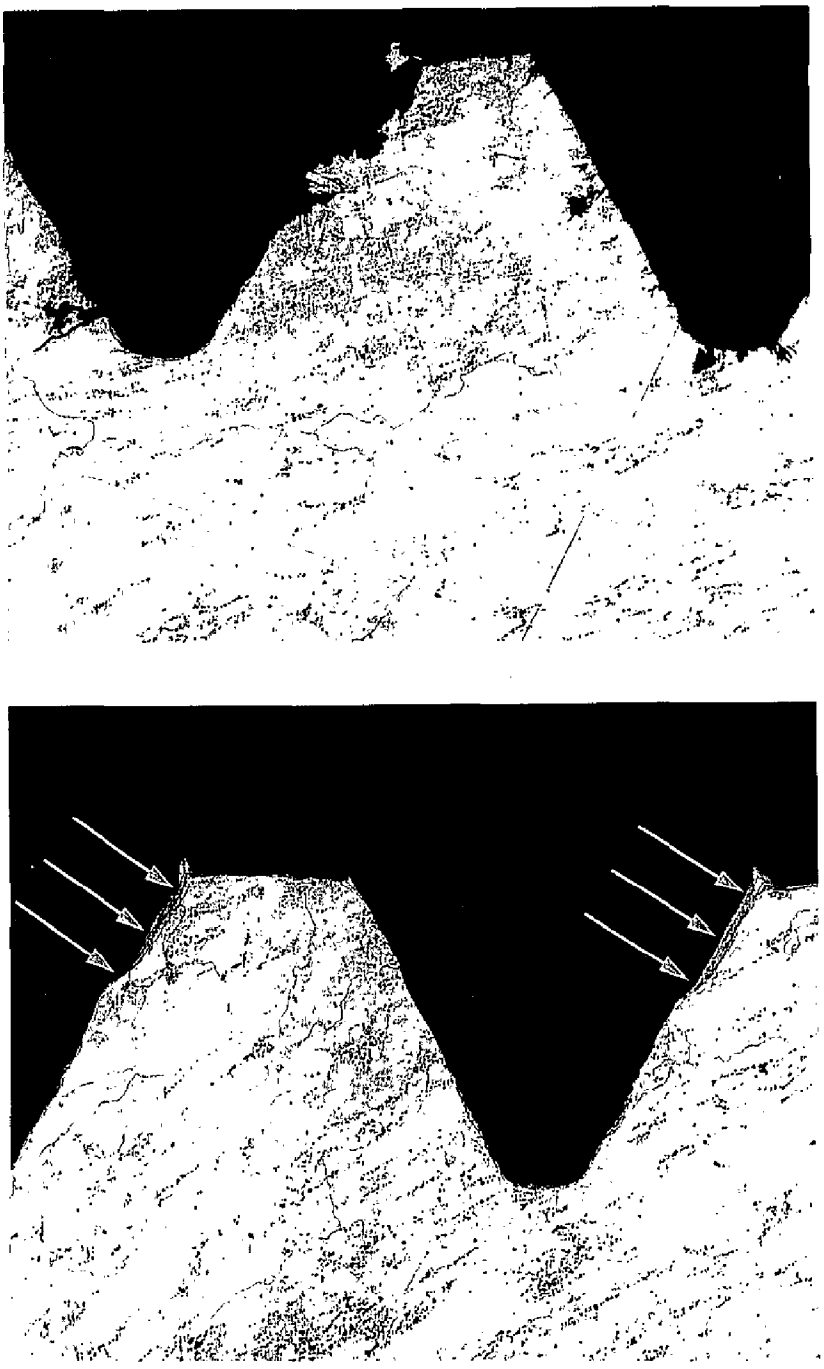

Figure 49. Same section as Figure 48, but at end of threaded area exhibiting corrosion attack normal to thread surface and along grain boundaries. Note cold worked areas (arrows) in terminal threads that typically indicate mismatching of threads, 1% NaOH etchant, X50.

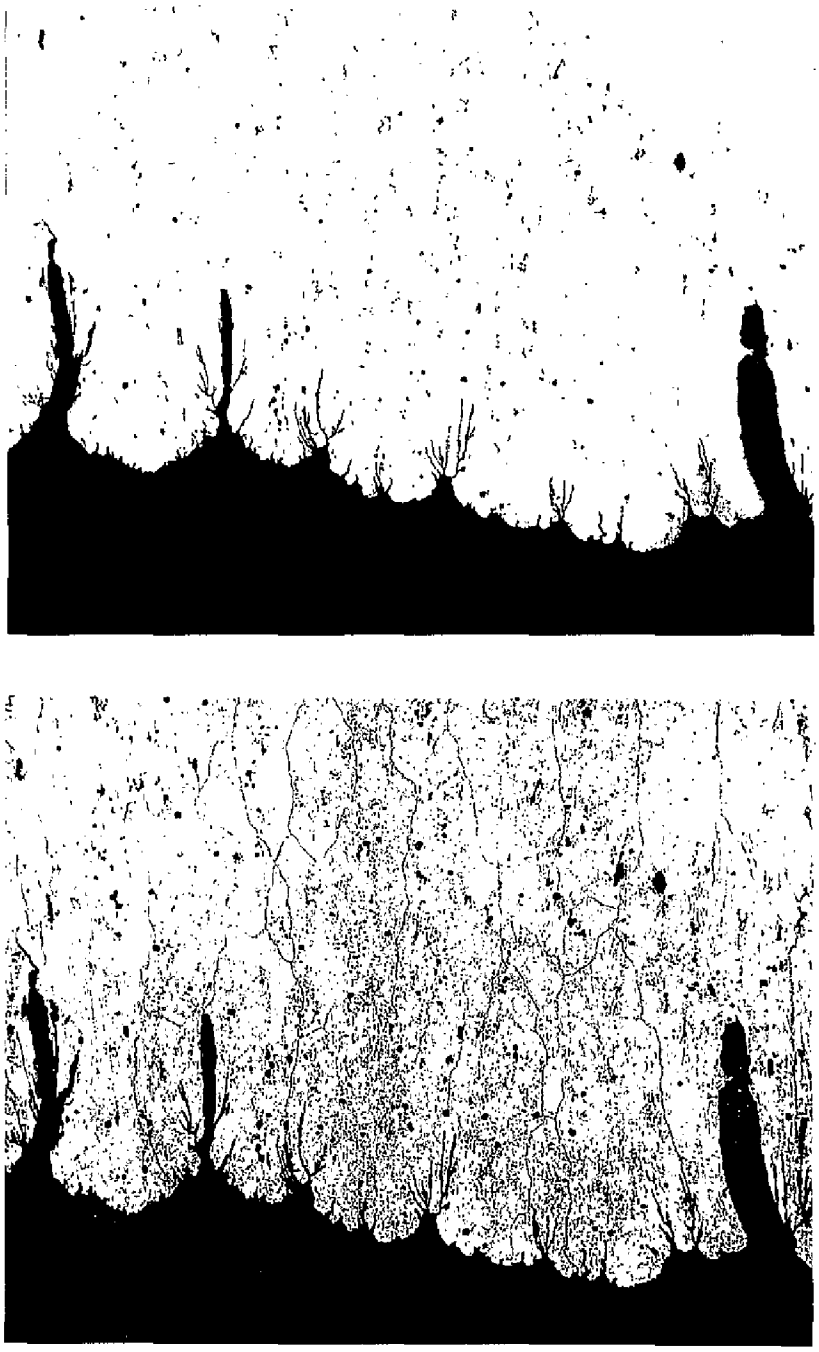

Figure 50. Longitudinal section behind threads and intersecting with wrinkled interior surface below threads (see Figure 8) revealing cracks emanating from surface texture notches, high apparent inclusion content, and large recrystallized grains; top, as-polished; bottom, 1% NaOH etchant; X100.

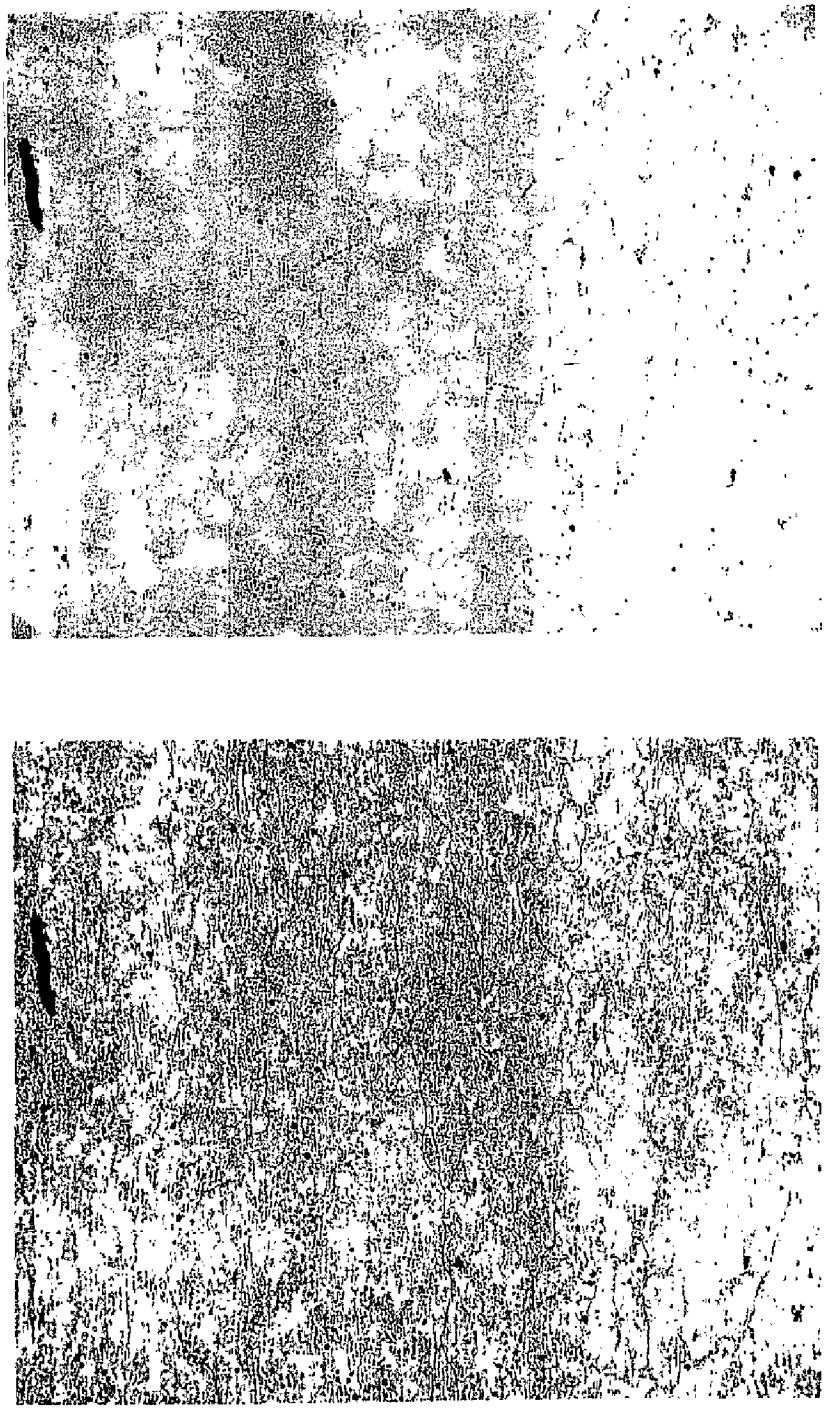

Figure 51. Same plane as Figure 50, but at level of bottom thread revealing a slight increase in micro-constituent alignment; top, as-polished; bottom, 1% NaOH etchant; X100.

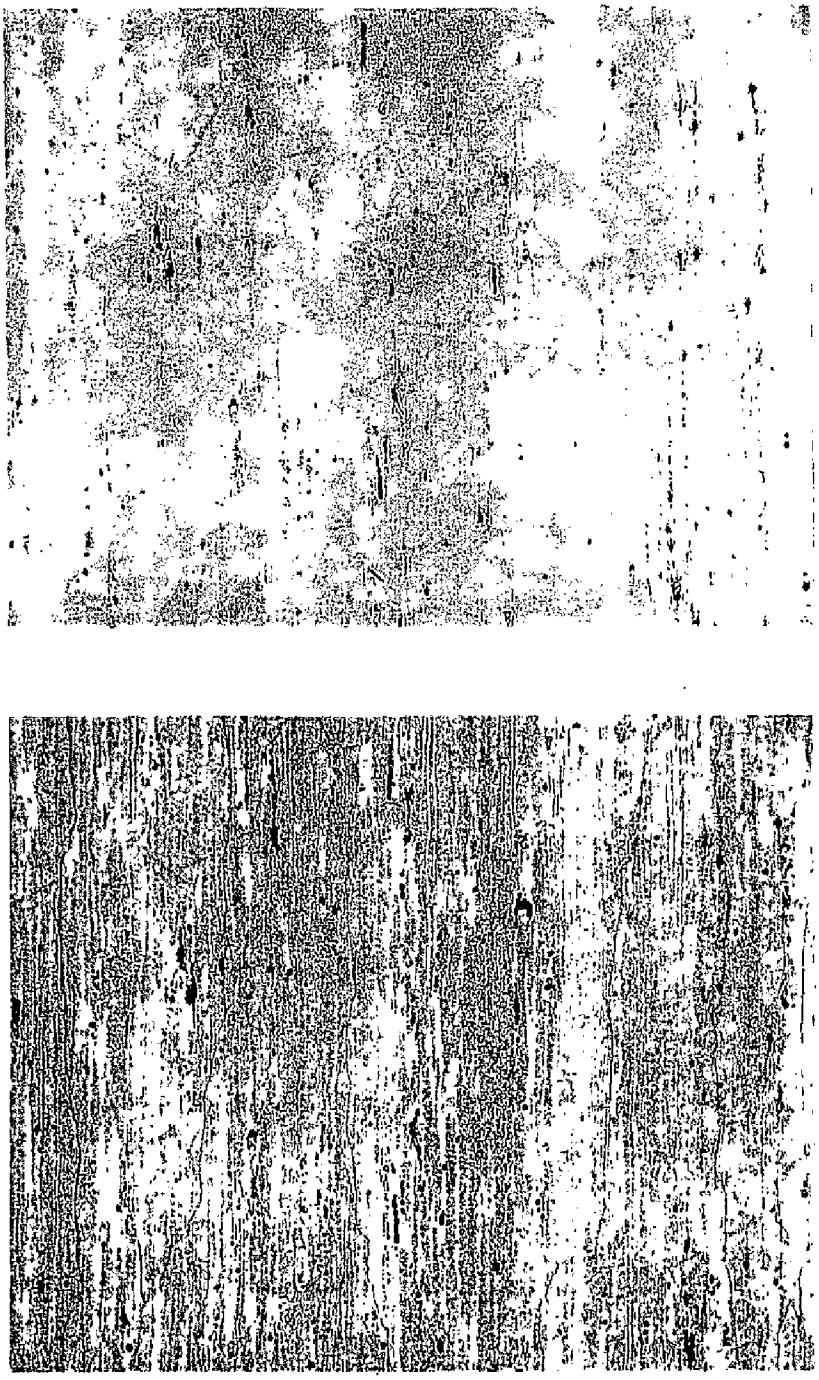

Figure 52. Same plane as Figure 50, but at level of top thread revealing a highly aligned microstructure and a very large elongated grain structure; top, as-polished; bottom, 1% NaOH etchant, X100.

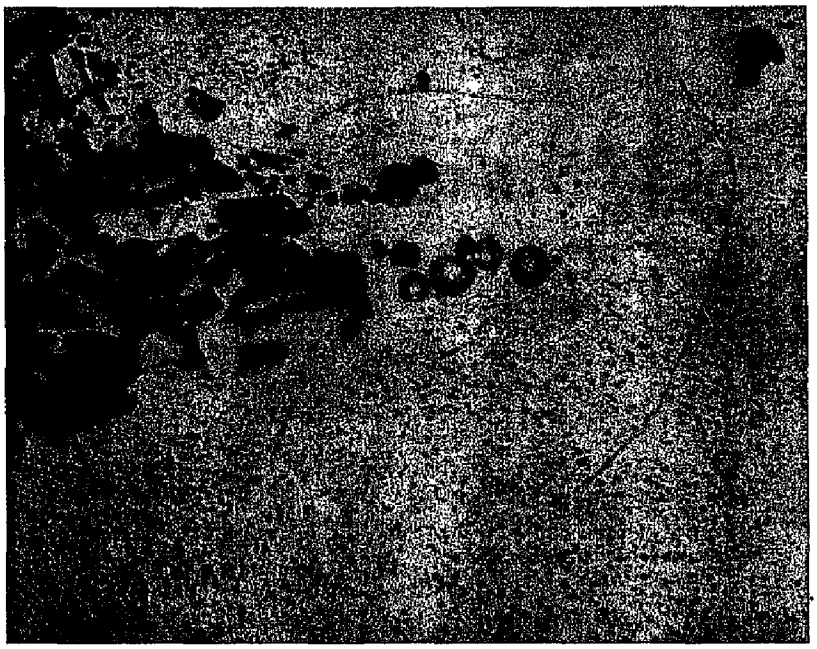

Figure 53. Stacking of microconstituents and unidentified inclusions observed in the radial section approximately 1/8 inch distant from heavy wall fracture surface common to fracture pieces (1I) and (4), 1% NaOH etchant, X1000.